Marine and Petroleum Geology 122 (2020) 104665

Contents lists available at ScienceDirect

Marine and Petroleum Geology

journal homepage: www.elsevier.com/locate/marpetgeo

Research paper

Organic-rich shale caprock properties of potential CO_2 storage sites in the northern North Sea, offshore Norway

Md Jamilur Rahman [a,*], Manzar Fawad [a], Nazmul Haque Mondol [a,b]

[a] Department of Geosciences, University of Oslo (UiO), Sem Sælands Vei 1, 0371, Oslo, Norway
[b] Norwegian Geotechnical Institute (NGI), Sognsveien 72, 0806, Oslo, Norway

ARTICLE INFO

Keywords:
Organic-rich shale
Caprock properties
Rock brittleness
Compaction
Rock physics analysis
Northern North Sea

ABSTRACT

Assessment of the geomechanical properties of organic-rich shale caprocks is critical for a successful CO_2 storage into a saline aquifer. In this study, we investigated the geochemical properties of the organic-rich shale caprocks of the Draupne and Heather formations, overlying the potential sandstone reservoirs of Sognefjord, Fensfjord, and Krossfjord formations in the northern North Sea, offshore Norway. The caprock's depositional variations within the sub-basins are established by analyzing the gamma-ray shape and stacking patterns. The effect due to differences in depositional environments, on the caprock compaction behavior is investigated by integrating petrographical analysis of core and cutting samples from 3 wells and by rock physical analysis of wireline log data from 27 exploration wells. Three rock physics templates are used where the wireline log data are interpreted using the published background trends. The effect of kerogen type, maturation level, and deposition environment on caprock properties within the study area are also evaluated. Moreover, the caprock property, such as brittleness, is estimated by using four mineralogy and elastic property-based, empirical relations, which is a quantitative measure of caprock property with respect to changes in stress-state. Finally, the seismic inversion method is assessed for the possibility of extracting caprock properties from surface seismic data. Regardless of compaction processes, the results indicate that the Heather Formation is mechanically stronger than the Draupne Formation. However, both formations appear to be ductile in nature. The depositional environments control the mineralogical composition and fabric of the Draupne and Heather formations, which influence the caprock properties significantly. Results also show that the effect of TOC on caprock properties is insignificant in the study area. The brittleness of the organic-rich shale caprocks in the study area follows a different trend compared to the published trends. We also observed an excellent correlation between the log-derived elastic properties and geomechanical parameters. Still, it is difficult to assess the caprock elastic properties from seismic due to the overlap of data clusters. The evaluation of caprock geomechanical behaviors is challenging as these properties are site-specific and also influenced by other factors such as exhumation, in-situ stress conditions, the existence of natural fractures, and their orientations.

1. Introduction

Geological storage of human-generated CO_2 into a saline aquifer is one of the many solutions for reducing CO_2 impact on the atmosphere. Norwegian Government has developed a strategy for large scale CCS (carbon capture and storage) as the necessity of it is already well documented by the UN's climate panel (IPCC) and International Energy Agency (IEA). Partnership with the industries, the government is interested in defining the best possible sites for sequestrating CO_2 into the subsurface in the Norwegian Continental Shelf (NCS). Smeaheia is one of the potential storage sites evaluated by Equinor and Gassonova, which is located in the eastern part of the northern North Sea (Fig. 1). The structures within the Semaheia area are mainly fault-bounded three-way closures with thin organic-rich shale caprocks. Troll Oil/Gas Field located west of Smeaheia, has oil and gas production from the same-targeted reservoirs. There is a possibility of lateral connectivity between Smeaheia, and the Troll Field that has been considered a potential risk. Moreover, this area has experienced several stages of rifting events (Faleide et al., 2015), following the collapse of Caledonian Orogeny in the Devonian time (Fossen and Hurich, 2005; Gabrielsen et al., 2010),

* Corresponding author.
E-mail addresses: m.j.rahman@geo.uio.no (M.J. Rahman), manzar.fawad@geo.uio.no (M. Fawad), nazmulh@geo.uio.no (N.H. Mondol).

https://doi.org/10.1016/j.marpetgeo.2020.104665
Received 7 May 2020; Received in revised form 15 August 2020; Accepted 17 August 2020
Available online 19 August 2020

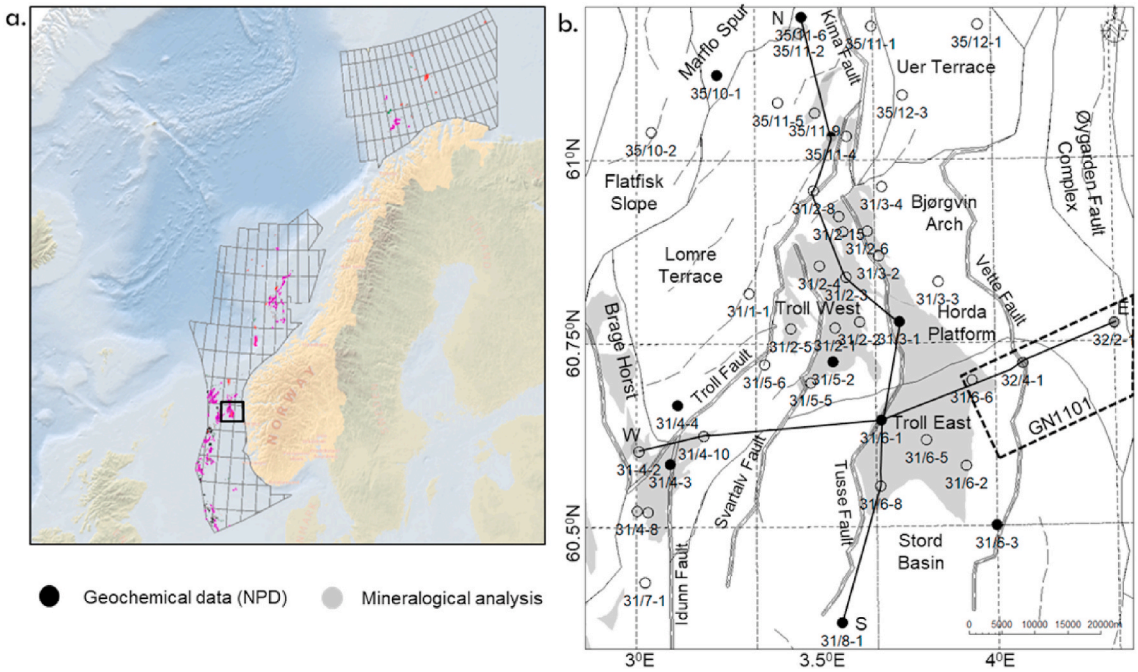

Fig. 1. a) The rectangle shows the study area on the Norwegian Continental Shelf, b) The locations of the studied wells correspond to the structural elements and major faults. The grey shaded areas are the hydrocarbon discoveries within the study area. The GN1101 3D seismic survey is outlined with a stippled rectangle, and the black lines represent the N–S and E-W well correlations presented in Fig. 2.

which leads to forming several large scale faults penetrating through the reservoir and caprocks up to the overburden. Therefore, careful investigations of caprock properties are necessary to prevent any CO_2 leakage risk.

In the study area, the main reservoir sandstones are the Jurassic Sognefjord, Fensfjord and Krossfjord formations, and organic-rich Draupne and Heather formations act as the primary seal. The thickness of caprocks varies significantly. One of the critical factors for CO_2 injection within a saline reservoir is the change in pore pressure, which ultimately changes the state of effective stress (i.e., principal stress minus pore pressure) and controls deformation and failure of reservoir-caprock pairs (Verdon et al., 2013). Additional, hydrological and geochemical processes influence the effective stress, potentially affecting the geomechanical properties of caprocks (Norton, 1984; Johnson et al., 2004; Shell, 2014). A potential consequence is the shear fracture or failure of caprock when shear stress exceeds the shear strength. This event not only depends on failure criteria but also controlled by the ductility or brittleness of the caprock (Nygård et al., 2006). This geomechanical properties (brittleness or ductility) of caprock is a complex function of rock lithology, texture, effective stress, temperature, strength, fluid type (Handin and Hagar, 1957; Davis and Reynolds, 1996; Nygård et al., 2006), diagenesis, TOC maturation, etc. (Walles, 2004). Additionally, natural fractures and planes of weakness can also affect these properties (Gale et al., 2007). Soft clay and organic matter (OM) cause a reduction in velocities and Young's modulus (E) while increasing the Poisson's ratio (PR) whereas stiff minerals (i.e., quartz, feldspar, pyrite, and carbonate) increase velocities and E with decreasing PR (Aoudia et al., 2010). The depth of burial can have both positive and negative effects on rock brittleness. An increase in depth generally increases pressure and temperature; hence the increase in the degree of compaction, along with the alteration of organic matter to enhance the brittleness. Furthermore, the silica enrichment due to clay mineral alteration with depth increase brittleness (Walles, 2004). Brittle deformation more likely occurs when a material is stiff and has higher shear strength. Thus, lithified shales are more fragile than young and uncemented mudrocks (Nygård et al., 2006). Rocks with certain mineralogy have less effect on brittleness with increasing pressure and temperature (Wang and Gale, 2009). However, all processes that govern the caprock properties are very complicated and depend on the depositional and diagenetic processes. Therefore, it is crucial to evaluate the geomechanical properties of organic-rich shale caprock (ORSC) in the study area for successful CO_2 sequestration.

In this study, we evaluate the rock compositional variation and the subsequent effect on elastic and geomechanical properties of the ORSC of Draupne and Heather formations in the northern North Sea, offshore Norway. The aim is to identify the caprock depositional and compaction processes variations by petrographic, petrophysical, rock physical and geophysical interpretations and find out the possible correlation between properties. The local depositional variation is identified using the differences in gamma-ray responses. Depositional processes are the critical factor for the mineralogy and fabric changes (i.e., grain size, shape, sorting, etc.) within sub-basin, which influence the property of caprocks. The properties are altered just after the deposition by compaction processes (i.e., mechanical and chemical compaction). The depositional variation is validated by petrographic analysis (XRD; SEM and thin section), while the compaction effects are analyzed by three rock physics templates (Vp-Density; E-PR and LambdaRho-MuRho). The influence of TOC on caprock properties is also evaluated by analyzing maturation, type, and distribution of organic matter. Moreover, the geomechanical properties of the caprock are assessed by analyzing the brittleness indices values calculated both from mineralogical composition and elastic properties. Finally, a qualitative evaluation between the inverted acoustic impedance (AI) from seismic data and log-derived elastic, and geomechanical properties are accomplished to assess the possibility of extracting caprock geomechanical properties from the seismic data. The caprocks property (i.e., ductility/brittleness) in the study area is established by integrating all these analyses, which is a crucial parameter to evaluate the caprock's sealing potential.

2. Lithostratigraphy and structural setting

The Late Jurassic Heather Formation shale is a part of the Viking Group that overlying and interfingering with Krossfjord, Fensfjord, and Sognefjornd formation sandstones of the Brent Group (Fig. 2a). Heather

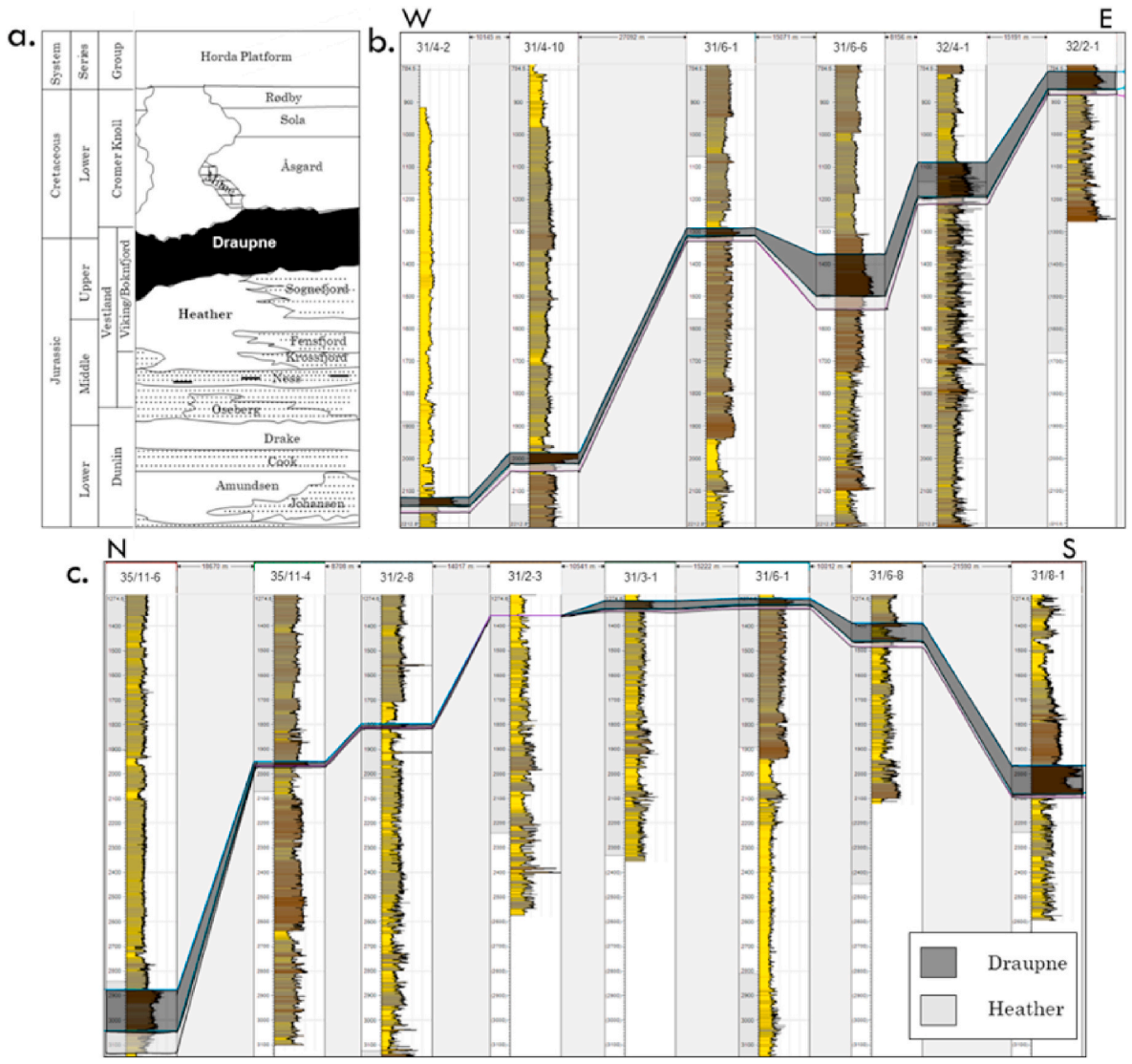

Fig. 2. a) A generalized Jurassic and Cretaceous stratigraphic succession in the study area (modified from NPD CO_2 Atlas, 2014). Well correlations along the b) E-W and c) N–S lines (Fig. 1) show the present-day depth variations of Draupne and Heather formations within the study area. Note that both correlations have vertical scale differences.

Formation consists of mainly grey silty claystone with thin streaks of limestone deposited in an open marine environment (NPD, 2020). On the Horda Platform, this unit interdigitates with the Middle Jurassic sandstones (Krossfjord, Fensfjord, and Sognefjord formations), where it sometimes becomes highly micaceous and may grade into sandy siltstone. Heather Formation also has significant thickness variations within the study area ranging between 0 and 159 m (Table 1). Stewart et al. (1995) divided Heather Formation in the Horda Platform area into three sub-units (A, B, and C). In this study, we evaluate only the Heather C unit, which is sandwiched between the Sognefjord and Draupne formations.

The Draupne Formation shale is also a part of the Viking Group, deposited in the Late Jurassic time within the East Shetland Basin, the Viking Graben, and over the Horda Platform area (NPD CO_2 atlas, 2014). The thickness of Draupne Formation varies significantly within the study area, ranges from 0 to 159 m (Table 1). The Draupne Formation consists of dark grey-brown to black, usually non-calcareous, carbonaceous, occasionally fissile claystone. It acts as the primary seal of the Middle Jurassic Sognefjord Formation sandstone reservoir. The formation was deposited in an open marine environment with restricted bottom circulation and often with anaerobic conditions (NPD, 2020), and characterized by high gamma-ray values (usually above 100 API) because of TOC and high Uranium content. Interbedded sandstone and siltstone, as well as minor limestone streaks and concretions, are also present. In the lower boundary, Draupne Formation generally has a diachronous contact with the Heather Formation. However, on the northern Horda Platform, Late Jurassic sandstones of Sognefjord Formation mark the base of the Draupne Formation. The upper boundary of the Draupne Formation is usually marked by Cretaceous rock (Cromer Knoll Group), which has a higher velocity and lower gamma-ray response than the over and underlying rocks (NPD, 2020).

The two main rifting events occurred in the Horda Platform area during the Permo-Triassic and the Late Jurassic to Mid-Cretaceous times (Whipp et al., 2014). During the 1st rifting event, a wide basin with deep-rooted faults and thick syn-depositional wedges was centered below the Horda Platform. However, Late Jurassic to Mid Cretaceous event shifted westward with major rifting and tilting observed in Lomre Terrace in the Late Jurassic (Stewart et al., 1995) and weak stretching on the Horda Platform itself (Roberts et al., 1993, 2019; Færseth, 1997; Whipp et al., 2014). The study area consists of several N–S trending faults (Fig. 1b), which are believed to be rooted in Caledonian zones of crustal weakness (Whipp et al., 2014). These faults also demarcate the

Table 1
Maximum burial depth, present depth, and thickness of Draupne and Heather formations penetrated by the studied wells. The structural elements as suggested by NPD (2020).

Well name	Structural Elements (NPD)	Draupne Formation top depth (m BSF)		Thickness (m) Draupne	Heather[b] Formation top depth (m BSF)		Thickness (m) Heather
		Present	Max.[c]		Present	Max.[c]	
31/2-1	Bjørgvin Arch	1066	1186	26	1092	1212	0
31/2-2		1126	1256	63	1189	1319	0
31/2-3		1023	1413	0	1023	1413	0
31/2-4		1004	1264	0	1004	1264	0
31/2-5		1171	1411	0	1171	1411	0
31/2-6		1113	1483	11	1124	1494	0
31/2-8		1451	1681	16	1467	1697	0
31/2-15		1147	1417	0	1147	1417	0
31/2-18		1163	1443	0	1163	1443	0
31/3-1		963	1343	32	995	1375	9
31/3-2		1176	1496	26	1202	1522	0
31/3-3		1193	1713	49	1242	1762	10
31/3-4		1247	1577	23	1270	1600	0
31/4-3		1815	1985	8	1823	1993	0
31/4-6		1968	2118	13	1981	2131	14
31/4-8		1936	2076	3	1939	2079	0
31/4-10		1749	1869	20	1769	1889	0
31/5-2		1133	1323	41	1174	1364	6
31/5-5		1224	1444	0	1224	1444	0
31/5-6		1441	1646	3	1444	1649	0
31/7-1		2000	2150	11	2011	2161	0
32/2-1		453	1253	54	508	1308	17
35/11-7		1409	1604	3	1412	1607	0
31/6-1	Stord Basin	986	1316	25	1011	1341	14
31/6-2		996	1456	113	1109	1569	25
31/6-3		1044	1474	125	1169	1599	16
31/6-5		1061	1451	92	1153	1543	38
31/6-6		1056	1526	129	1185	1655	40
31/6-8		1087	1417	73	1160	1490	22
31/8-1		1664	1914	110	1774	2024	14
32/4-1		774	1474	106	880	1580	23
31/1-1	Lomre Terrace	1685	1885	3	1688	1888	0
31/4-4		2061	2181	65	2126	2246	0
35/11-2		2532	2692	115	2647	2807	128
35/11-4		1594	1784	18	1612	1802	0
35/11-5		2298	2478	129	2428	2608	65
35/11-6		2505	2655	159	2664	2814	96
35/11-9		2003	2183	150	2153	2333	17
31-4-2	Brage Host	1979	2139	25	2004	2164	19
35/10-1	Marflo Spur	2714	2854	48	2762	2902	118
35/10-2	Flatfisk Slope	3525	3650	97	3622	3747	131
35/11-1	Reggeteinen Ridge	1633	1963	0	1633	1963	95
35/12-1	Uer Terrace	1984	2464	37	2021	2501	159
35/12-3		1638	1998	14	1652	2012	13

[c] Corrected for exhumation estimated from Vp-Depth trend to represent the maximum burial depth.
[b] Only considered interval between Draupne and top reservoirs section.

structural elements interpreted by NPD (2020). For example, the Horda Platform (Bjørvin Arch and Stord Basin) is separated by the Troll fault complex in the west and Øygarden fault complex in the east. Moreover, the faults Vette, Tusse, and Svart created compartmentalization within the Horda Platform, which separated Troll East and West Fields (Fig. 1b). Other major faults like Kima, Brage, Idunn fault complexes, and minor faults also played an essential role during structural deformation within the study area. Uplifted blocks acted as provenance to fill the accommodation spaces created by rifting and then following the thermal subsidence (Jordt et al., 1995; Anell et al., 2009; Faleide et al., 2015).

The structural well correlations show the present-day depth difference of Draupne and Heather formations within the studied wells (Fig. 2b&c). In the middle of the study area (crossing Troll East), both formations are gradually going deeper from east to west with varying thickness. In contrast, the N–S correlation shows that the Draupne and Heather formations deepen in both north and south direction, with the northern well (Lomre Terrace) being deeper than the southern well (Stord Basin). The wells with the shallowest reservoir lie in the center (Bjørgvin Arch) containing very thin or no Draupne and Heather formations.

The study area became tectonically active during Late Jurassic time when the Draupne and Heather formations were deposited. The major faults rotated as a result of the basement blocks' rotation produced numerous local basins (Faleide et al., 2015), which lead to forming a high energy ribbon trending NNE-SSW along the present Troll West area following the Troll fault zone. This trend is gradually prograding north-westward and crosses the main boundary fault (Troll fault) into the Lomre Terrace. Moreover, the Horda Platform has tilted towards the east during the Late Kimmeridgian time, which resulted in NNE-SSW zero thickness trend, and thin Heather deposited into the Troll East because of sediment bypassed into the Lomre Terrace area (Stewart et al., 1995). This zero thickness bypass or erosional trend is also found in Draupne and Heather formation's thickness maps (Fig. 5), which reveals that during transgression, the erosional/non-depositional structural high on top of Troll West existed and influences the sedimentation in the study area.

Table 2
Summary of the TOC and R_0 from the available well reports (NPD, 2020). The corresponding log derived TOC is also shown for comparison.

Formation	Well name	Structural Elements	TOC (wt%) rock-eval			TOC (wt%) log[c]		R0 (%)	
			Mean	STD	N	Mean	STD	Mean	STD
Draupne	31/3-1	Bjørgvin Arch	3.03	0.47	4	3.12	0.89	0.41	0.06
	31/5-2		2.62	1.21	7	2.57	1.21	–	–
	31/4-3		5.71	1.00	1	5.19	2.24	0.33	–
	31/8-1	Stord Basin	3.35	1.78	12	3.50	1.74	0.36	0.02
	31/6-1		1.63	0.10	3	1.47	1.36	0.42	0.00
	31/6-3		1.47	1.04	9	1.75	2.37	0.55	0.04
	31/4-4	Lomre Terrace	2.71	2.26	3	2.18	1.94	–	–
	35/11-4		0.71	1.05	6	1.01	0.64	0.45	0.05
	35/11-6		3.77	0.55	7	4.18	2.01	–	–
	35/10-1	Marflo Spur	3.93	1.27	4	4.29	2.88	–	–
Heather	31/8-1	Stord Basin	6.18	1.30	2	4.92	0.57	–	–
	31/6-1		2.62	0.25	2	0.93	1.28	–	–
	35/11-6	Lomre Terrace	3.60	0.80	4	3.20	3.14	–	–
	35/10-1	Marflo Spur	3.56	0.50	8	3.82	1.49	–	–

Mean (Harmonic); STD – Standard deviation; n – number of readings.
[c] Predicted using equation 1.

3. Database and methods

The log-derived elastic properties can reveal the compaction history of a caprock. Moreover, the correlation between the present-day caprock properties and the paleo-depositional history can be illustrated by analyzing the petrographical images. However, the compaction processes are too complicated due to the influence of several factors (i.e., tectonics, sea-level fluctuation, initial pore-water chemistry, etc.), which can be very difficult to predict. We utilized the data from 44 exploration wells (Fig. 1) from the study area to evaluate Draupne and Heather formations caprock properties. Table 1 shows the available wells and structural setup; these wells represent the exhumation and thickness of Draupne and Heather formations. The majority of the wells (i.e., 31) are from the Horda Platform area (i.e., Bjørgvin Arch and Stord Basin); however, the remaining wells are the control points for other structural elements such as Lomre Terrace, Uer Terrace, Brage Host, Marflo Spur, Flatfisk Slope, and Reggeteinen Ridge. All the wells were used in the thickness map generation process, while 27 wells were selected based on Draupne Formation thickness (>10 m) and available logs (i.e., gamma-ray, density, p-sonic, resistivity, neutron porosity, etc.) for physical and mechanical property evaluation. Moreover, 10 wells out of 44 have available geochemical data (NPD, 2020), which were used to evaluate TOC maturation in the study area (Table 2). Also, three wells (32/2–1, 32/4–1 & 35/11–4) that have the core and cutting samples within the caprock intervals were selected for petrographic study and grain size analysis.

3.1. Paleo-depositional environment and petrographic analysis

The gamma-ray log signatures help to identify the sea-level fluctuations and paleo-depositional variations within the local sub-basins. These depositional variations affect the rock properties during diagenesis (mechanical and chemical compactions). A funnel-shaped log curve in shallow marine setup reflects an upward increase in depositional energy with shallowing upward and coarsening while a bell shape replicates upward fining with a decrease in energy. However, a block shape curve represents the minimal fluctuation of depositional energy (Emery and Myers, 1995). Moreover, the vertical stacking pattern of the gamma-ray log curve reveals the paleo depositional relation between accommodation spaces and sediment supply rates (Van Wagoner et al., 1988).

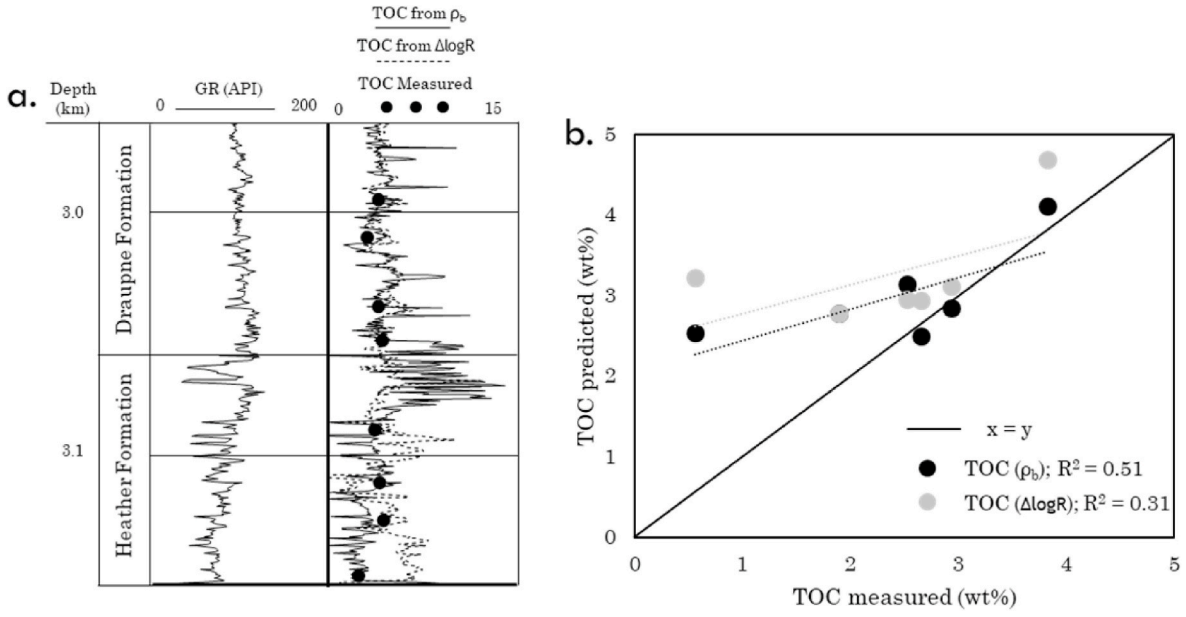

Fig. 3. a) Comparison of predicted TOC with the measured TOC (black dots; NPD, 2020) of Draupne and Heather formations in well 35/11–6. Calculations from ΔlogR method (Passey et al., 1990) are represented by the dotted line and from equation (1) using the bulk density by a solid line. The gamma-ray shows the variation with depth. b) Measured versus predicted TOC of the same data points show the correlation coefficient of two methods.

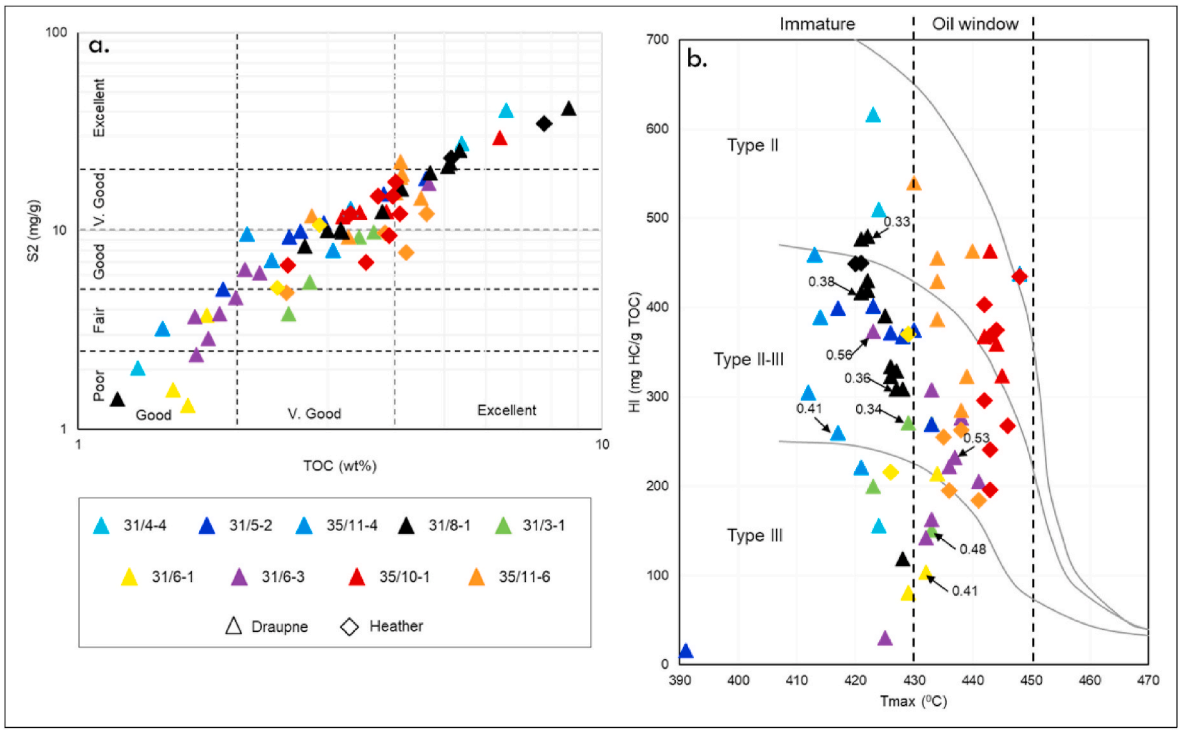

Fig. 4. a) Cross-plot of TOC versus S2 of Draupne and Heather formations showing the quality of the organic matter in the study area. The background template is modified after Peter (1986). (b) Pyrolysis T_{max} versus Hydrogen Index (HI) of Draupne and Heather formations from ten wells in the northern North Sea, showing the kerogen type and thermal maturity, according to Hunt (1996). It also indicates the associated vitrinite reflectance (R_o%) readings from NPD (2020).

Accommodation spaces, however, are a result of sea-level fluctuation and paleo tectonic activity while sediment supply depends on the sediment sources and weathering processes. Therefore, the log shape and variations of the stacking pattern of Draupne and Heather formations within the study area were analyzed to evaluate the depositional differences within the sub-basins. This paleo-depositional analysis is later validated using the petrographic interpretation. The interpretation of mineral fractions, grain sizes, and textural contrast was investigated by X-Ray diffraction (XRD), scanning electron microscope (SEM), and thin section analysis using the available core and cutting samples.

3.2. Geochemical data and TOC prediction

Organic matter types and maturation play vital roles for caprock properties; therefore, geochemical reports consisting of TOC (total organic carbon) data are scouted from the public domain database (NPD, 2020). Only 10 out of 44 wells have measured geochemical data; therefore, TOC for the rest of the wells was calculated using empirical relations (e.g., Passey et al., 1990; Vernik and Landis, 1996). Calculated TOC was calibrated with the laboratory-measured TOC acquired from the NPD (Norwegian Petroleum Directorate) database. Two methods were tested using the well 35/11-6 dataset, where the sonic and resistivity logs were used in the ΔlogR method (Meyer and Nederlof, 1984; Passey et al., 1990) and density log in equation (1) (Vernik and Landis, 1996; Carcione, 2000) to estimate TOC fractions. A comparison of predicted TOC using the two methods is shown in Fig. 3.

Both methods show reasonable estimation; however, density generated TOC fraction has a better match with measured data compared to ΔlogR method (Fig. 3b). Therefore, we calculated density based TOC for all the studied wells using the following equation:

$$TOC\ (wt\%) = a[\rho_k(\rho_m - \rho_b)]/[\rho_b(\rho_m - \rho_k)] \quad (1)$$

Where, ρ_k is the kerogen density that has a range of 1.1–1.6 g/cm^3 (Hansen et al., 2019) and it depends on the maturation of organic matter (Vernik and Landis, 1996; Passey et al., 2010; Vernik and Milovac, 2011; Alfred and Vernik, 2013; Dang et al., 2016); ρ_m is the matrix density which depends on the mineralogy, grain fabric and diagenesis, i.e., clay mineral transformation (Hart et al., 2013; Carcione and Avseth, 2015); ρ_b is the bulk density log, and 'a' is the constant which is related to the fraction of carbon in organic matter and can vary according to the maturation level. For example, Vernik and Landis (1996) assume a = 67, while a = 70–85 is suggested by Vernik and Milovac (2011).

In our calculation, the study area was subdivided into four zones based on the OM volume, type, and maturation. Overall the OM is type-II to type-III with immature in Horda platform area (i.e., Bjørgvin Arch and Stord Basin) and within the oil window in the deeper section in Lomre Terrace and Marflo Spur (Fig. 4). Based on this information, we fixed 'a' and ρ_k value for all the wells located in each sub-sections. Later, the matrix density (ρ_m) in equation (1) was used as the variable to get the best fit with measured TOC (Table 2). When there was a better match between the measured and calculated mean TOC values (Table 2), the same properties (i.e., 'a', ρ_k & ρ_m) used to calculate the TOC percentage for the rest of the wells (used the nearest measured well values).

3.3. Compaction and caprock properties

Caprock properties are varied significantly due to the maximum temperature and pressure it experienced. This whole rock compaction process was divided into zones where mechanical compaction is stress-dependent, and chemical compaction depends on temperature. Therefore, the estimation of maximum burial depth of the zones of interest is necessary. Hence, the exhumation and temperature of each studied wells were calculated. The normal compaction trend-based (NCT-based) exhumation estimation was carried out to evaluate the maximum burial of the caprocks (Table 1). The silt-kaolinite (50:50) normal compaction trend (NCT) suggested by Mondol (2009) was used to estimate the exhumation. The maximum burial depth calculated in this study was calibrated with the published literature (Baig et al., 2019). The temperature, however, estimated using BHT (bottom hole temperature) and TVD (total vertical depth) of the studied wells and denoted as:

Table 3
Present and maximum burial depth with the corresponding temperature of Draupne and Heather formations dividing the wells into three compaction clusters (MC, TZ, and CC).

	Well name	Draupne Formation				Heather Formation			
		Present Depth (m BSF)	P. Temp. (^{0}C)	Max.[a] Depth (m BSF)	M. Temp. (^{0}C)	Present Depth (m BSF)	P. Temp. (^{0}C)	Max.[a] Depth (m BSF)	M. Temp. (^{0}C)
MC	32/2-1	453	15.9	1253	43.9	508	17.8	1308	45.8
	32/4-1	774	27.1	1474	51.6	880	30.8	1580	55.3
	31/3-1	963	33.7	1343	47.0	995	34.8	1375	48.1
	31/6-1	986	34.5	1316	46.1	1011	35.4	1341	46.9
	31/6-2	996	34.9	1456	51.0	1109	38.8	1569	54.9
	31/6-3	1044	36.5	1474	51.6	1169	40.9	1599	56.0
	31/6-6	1056	37.0	1526	53.4	1185	41.5	1655	57.9
	31/6-5	1061	37.1	1451	50.8	1153	40.4	1543	54.0
	31/2-1	1066	37.3	1186	41.5	1092	38.2	1212	42.4
	31/6-8	1087	38.0	1417	49.6	1160	40.6	1490	52.2
	31/2-2	1126	39.4	1256	44.0	1189	41.6	1319	46.2
	31/5-2	1133	39.7	1323	46.3	1174	41.1	1364	47.7
	31/3-2	1176	41.2	1496	52.4	1202	42.1	1522	53.3
	31/3-3	1193	41.8	1713	60.0	1242	43.5	1762	61.7
	31/2-8	1451	50.8	1681	58.8	1467	51.3	1697	59.4
	35/11-4	1594	55.8	1784	62.4	1612	56.4	1802	63.1
	31/8-1	1664	58.2	1914	67.0	1774	62.1	2024	70.8
	31/4-10	1749	61.2	1869	65.4	1769	61.9	1889	66.1
	31/4-3	1815	63.5	1985	69.5	1823	63.8	1993	69.8
TZ	31/4-6	1968	68.9	2118	74.1	1981	69.3	2131	74.6
	31-4-2	1979	69.3	2139	74.9	2004	70.1	2164	75.7
	31/4-4	2061	72.1	2181	76.3	2126	74.4	2246	78.6
CC	35/11-5	2298	80.4	2478	86.7	2428	85.0	2608	91.3
	35/11-6	2505	87.7	2655	92.9	2664	93.2	2814	98.5
	35/11-2	2532	88.6	2692	94.2	2647	92.6	2807	98.2
	35/10-1	2714	95.0	2854	99.9	2762	96.7	2902	101.6

Temperature were calculated using the aveargе temperature gradient (35^{0}C/KM).
[a] Corrected for exhumation estimated from Vp-Depth trend to represent the maximum burial depth.

$$m = \frac{(y - c)}{TD} \quad (2)$$

where m is thermal gradient, y is bottom hole temperature, c is mean annual temperature at the seafloor, and TD is the total depth below the seafloor. We used 5 °C as mean annual temperature for the study area.

Based on the exhumation and corresponding maximum burial/temperature, Draupne and Heather formations were divided into three subgroups: i) MC-mechanically compacted, ii) TZ-transition zone, and iii) CC-chemically compacted. As TZ is a range instead of a single value, we defined 65–75 °C as the TZ for the study area (Table 3). The P-wave velocity (Vp) versus density (ρ) template is a good tool for acoustic property characterization where the background curves (i.e., friable sand model, 20%, 50%, 80% and 100% clay volume curves) were adapted from Avseth et al. (2005). This model called the Dvorkin-Gutierrez silty shale model, where the saturated elastic moduli of shale were estimated by using the Hashin-Shtrikman lower bound as a function of clay content, assuming the adding silt grains consist of 100% quartz (Avseth et al., 2005). Moreover, the effect of the volume of shale within the caprocks was assessed by comparing the volume of clay (Vsh) data points with the background curves. Though the gamma-ray (GR) is the proxy for the volume of clay in any formation, the GR values also depend on many other factors. We calculated the volume of shale (Vsh) from the gamma-ray log using Larionov's (1969) younger (MC zone wells) and older (CC zone wells) rock equations. The elastic properties such as Young's Modulus (E), Poisson's Ratio (ν) and Lame parameters such as LambdaRho (λρ) and MuRho (μρ) was characterized using the templates where the background curves were adapted from Grieser and Bray (2007) and Perez and Marfurt (2014). These properties represent the geomechanical properties of the caprock under stresses, and for their calculations, P-wave velocity (Vp), S-wave velocity (Vs), and density are required. Vp and density are available, but Vs (shear wave velocity) is not recorded in any of the studied wells; therefore, we predict Vs using Random Forest (RF) - a machine learning algorithm. We tested several algorithms, where the RF yielded comparatively better results.

A prestack seismic inversion was also carried out for the 3D seismic volume GN1101 (Fig. 1b) covering the Smeaheia area (East of the study area) penetrated by two exploration wells (32/2–1 & 32/4–1). A set of five available partial stacks were used comprising angles 0–10°, 10–20°, 20–30°, 30–40°, and 40–50° to perform prestack inversion. Before extracting statistical wavelets from all the five partial stacks, a preconditioning alignment of traces using a non-rigid method (NRM) was carried out. Both the wells were correlated with seismic and obtained moderate to good correlation coefficient (0.6–0.7). Finally, the simultaneous inversion was applied to the partial stacks to obtain the acoustic impedance (AI) cube. The geometrical mean of AI value of Draupne and Heather formations was calculated using the surface attribute function.

3.4. Brittleness indices

The brittleness index (BI), which is the qualitative measure of rock behavior, was also estimated. The mineralogical composition of the caprocks significantly influences the geomechanical properties. The fraction of stiff minerals increases the caprock brittleness, while the ductile components decrease it. Several correlations are tested using published equations (Jarvie et al., 2007; Glorioso and Rattia, 2012; Alzahabi et al., 2015) within which Jarvie et al. (2007) equation (Eq. (3)) provide a better estimate of mineralogy-based brittleness index (MBI^1) for the studied caprocks:

$$MBI^1 = \frac{\text{Qtz}}{\text{Qtz} + \text{Carb} + \text{Cly}} \quad (3)$$

where Qtz is Quartz, Carb is Carbonate, and Cly is Clay. $MBI^1 = 1$ indicates brittle behavior, while $MBI^1 = 0$ represents the ductile behavior of the caprocks. It is noteworthy to mention that several authors considered dolomite (Wang and Gale, 2009), carbonate (Glorioso and Rattia, 2012), feldspar (Jin et al., 2014) and pyrite (Alzahabi et al.,

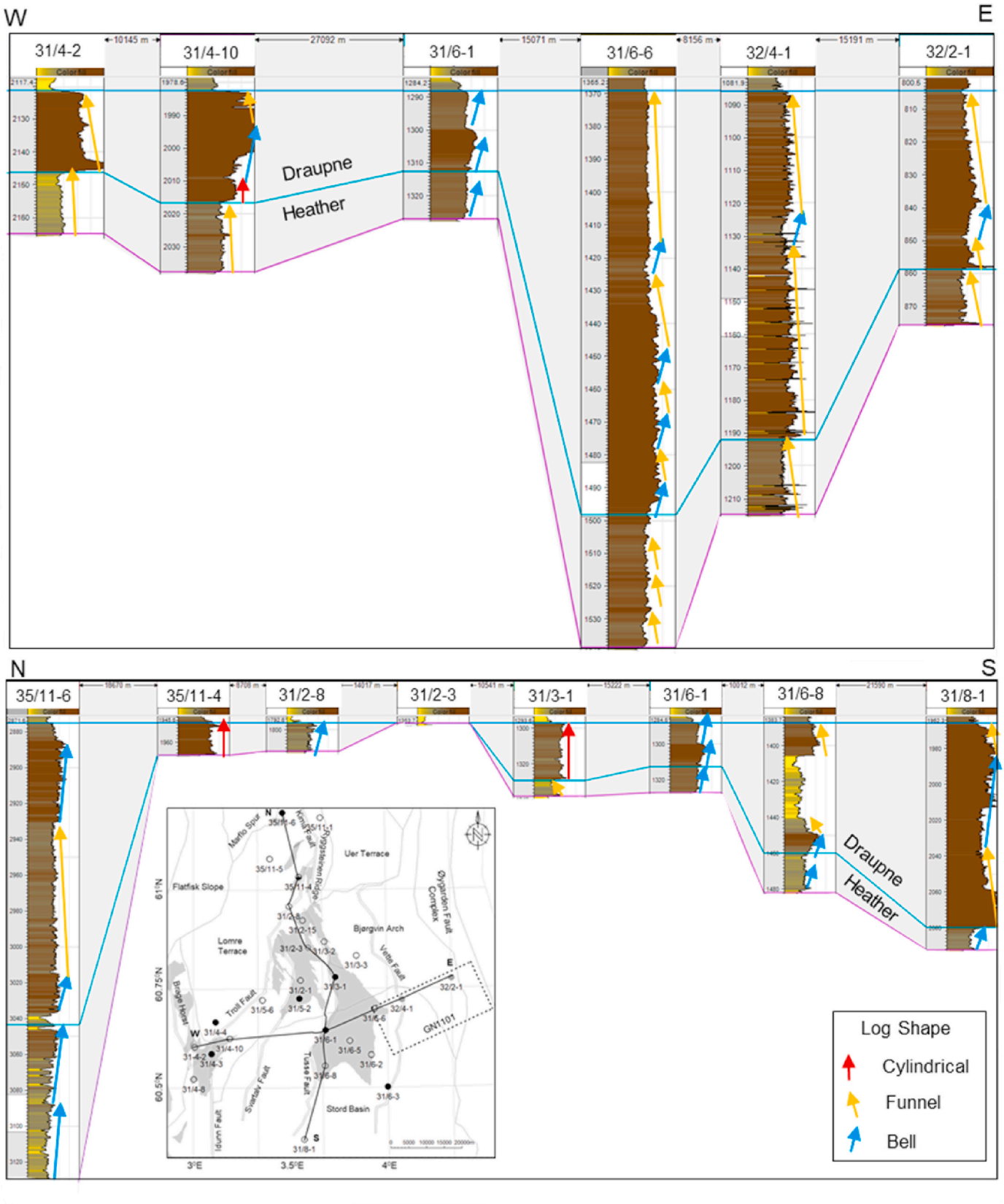

Fig. 5. Stratigraphic correlation along W-E and N–S cross-sections, flattened on top of the Draupne Formation showing the thickness variation with variable gamma-ray log patterns (cylindrical, funnel, and bell) in Draupne and Heather formations, which reveal the paleo-depositional changes. The insert map shows the profile locations and structural elements.

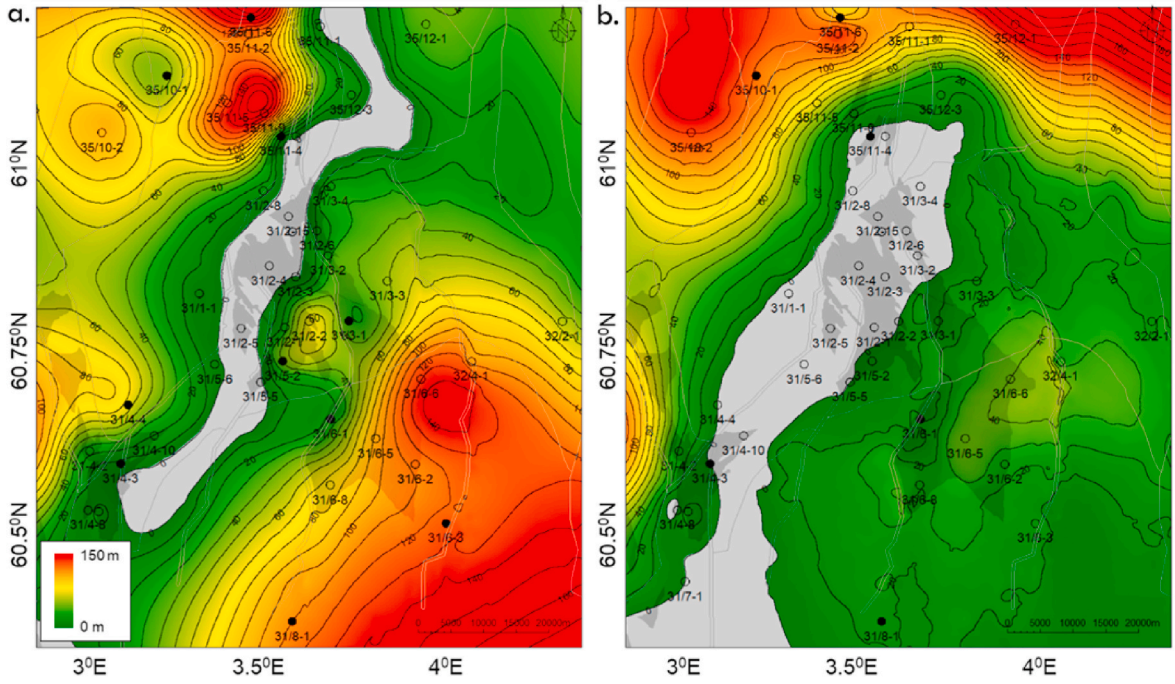

Fig. 6. The thickness maps generated from well log data for a) Draupne Formation and b) Heather Formation. A NNE-SSW zero thickness trend occurs in both formations. The contour intervals are 10 m in both maps.

2015; Rybacki et al., 2016) as stiff minerals while TOC (Wang and Gale, 2009) as a ductile component. Considering this, we modified equation (3) and proposed the following equation for mineralogy-based brittleness index (MBI^2):

$$MBI^2 = \frac{\text{Qtz} + \text{Carb} + \text{Fsp} + \text{Py}}{\text{Qtz} + \text{Carb} + \text{Fsp} + \text{Py} + \text{Cly} + \text{TOC}} \quad (4)$$

where Fsp is Feldspar, Py is Pyrite, and TOC is total organic carbon, and MBI^2 ranges between 0 (ductile) to 1 (brittle). Like MBI, elastic property based brittleness indices (EBI) are also available (i.e., Grieser and Bray, 2007; Rickman et al., 2008; Sharma and Chopra, 2012; Chen et al., 2014; Jin et al., 2014). We estimated the EBI using two elastic property-based empirical equations proposed by Grieser and Bray (2007) and Fawad and Mondol, 2020; unpublished, patent-pending on the procedure). The Grieser and Bray (2007) empirical equation is:

$$EBI^1 = \frac{1}{2}\left[\frac{E - E_{min}}{E_{max} - E_{min}} + \frac{\nu - \nu_{max}}{\nu_{min} - \nu_{max}}\right] \quad (5)$$

where E is static Young's modulus, E_{max} is 69 GPa, E_{min} is 0 GPa, and ν is static Poisson's ratio, ν_{max} is 0.5, ν_{min} is 0. Also, the higher the EBI^1 value is, the more brittle the caprock would be.

The log driven dynamic Young's modulus and Poisson's ratio were converted to log-based static values using Mullen et al. (2007) equation:

$$E_{stat} = \left[\frac{E_{dyn}}{3.3674}\right]^{2.042} \quad (6)$$

$$\nu_{stat} = \nu_{dyn} \quad (7)$$

The equation proposed by Fawad and Mondol (2020; unpublished, patent-pending on the procedure) is:

$$EBI^2 = \frac{0.00044AI - 1.3 - \sqrt{0.62\,\frac{R_W}{R_D}}\,(0.00019AI + 0.25)}{1.35 + 0.00028AI} \quad (8)$$

where AI is the acoustic impedance (g/cm^3×m/s); R_D is true formation resistivity (ohm-m), and R_W is the resistivity of pore water (ohm-m). Here we define the brittleness as an increase in stiffness of a rock due to compaction and addition of stiff mineral content (quartz, carbonate, or dolomite). Equation (8) is based on the physical and elastic properties of the organic matter (kerogen), quartz, and clay/water as end-members of a ternary model.

4. Results

4.1. Paleo depositional variation

The gamma-ray log shape is analyzed to identify the local depositional variations (i.e., facies changes) between the different sub-basins in the study area. The wells used for this analysis are carefully chosen so that all the structural elements (NPD, 2020) are represented, and the whole study area is covered. The N–S and W-E well sections (Fig. 5), consisting of 14 wells representing all the sub-basins, are used for this analysis. The number and type of log shapes vary within the wells and studied formations (i.e., Draupne and Heather). There is a sharp boundary observed between Heather and Draupne formations in wells (31/4–2, 31/4–10 & 31/8–1) in the SW part while more gradual changes observed in the rest of the study area (Fig. 5). The number of log cycles is thickness dependent. Wells, with a considerable thickness of Draupne and Heather formations, have more variety of patterns than the wells (31/2–8, 31/3–1, 31/4–2, and 35/11–4) penetrated thin sections mostly a single shape observed. The gamma-ray log shape patterns, however, do not follow any specific trend in some wells (such as wells 31/6–8 & 35/11-6 drilled in specific structural elements), which rather have a mixture of different patterns within the zones studied.

The gamma-ray values also show a considerable variation within the same formation as well as between Draupne and Heather formations. Generally, Heather Formation has low values of gamma-ray values compared to Draupne Formation, which might be an indication of the variation of depositional energy (i.e., higher energy leading to coarser grains in Heather Formation). However, depending on the locations and thickness, GR value varies significantly. The highest GR value in Draupne Formation is observed in the wells 31/4–2, 31/4–10, and 31/8–1. These wells are located within the south-western part of the study area covering part of the Stord Basin and Lomre Terrace. The lowest GR

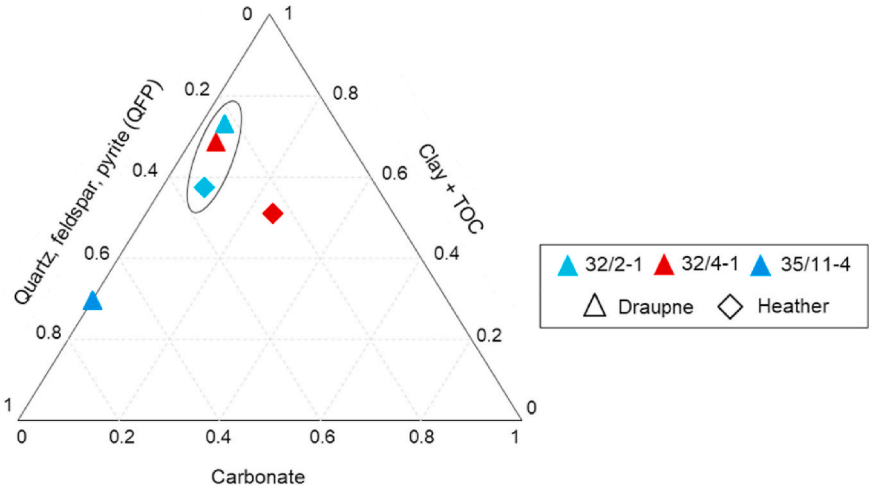

Fig. 7. The Ternary plot represents the compositional variability of Draupne and Heather formations within the three wells 32/2–1, 32/4–1, and 35/11–4. Note that carbonate minerals consist of calcite, dolomite, and siderite.

Table 4
Summary of bulk mineralogy and TOC of Draupne and Heather formations. Log-derived TOC is also shown for comparison.

Formation	Well no.	Mineralogy from XRD (wt%)					TOC[a]	TOC (wt%) log[b]	
		Quartz	Feldspar	Pyrite	Carbonate	Total Clay	(wt%)	Mean	STD
Draupne	32/2-1	18	4	1	5	70	2.81	2.26	1.31
	32/4-1	25	0	2	5	66	2.78	1.72	0.96
	35/11-4	43	6	22	0	28	2.08	1.01	0.64
Heather	32/2-1	24	10	1	8	55	2.64	1.63	0.54
	32/4-1	15	8	1	25	49	2.31	1.08	0.81

[a] TOC estimated from elementary study from the same core and cuttings used in XRD.
[b] Corrected for exhumation estimated from Vp-Depth trend to represent the maximum burial depth.

values are found near the Troll West area in well 31/2–8.

The paleo-depositional environment also affects the thickness of a formation. Along with sea-level fluctuation, thickness reflects the accommodation spaces and sediment supply during deposition. The thickness map reveals the paleo-depocenters within the study area. The thickness map of Draupne and Heather formations shows significant thickness variation with local depocenters within the study area (Fig. 6). Moreover, local highs and lows are following the fault orientation. The thickness of Draupne Formation ranges between 0 and 160 m, while it is 0–159 m in Heather Formation. A NE-SW zero thickness trend find following the Troll fault zone in both formations where the Troll fault is the boundary between the eastern platform area (Horda Platform) and the deep western basin (Viking Graben). The thickness of the Draupne Formation gradually increases in both NW and SE directions from the zero thickness trend. However, few local depocenters are also observed with higher thickness than the surroundings. In contrast, the thickness of Heather Formation increases towards West and NW direction (mainly in the deep basin area) while a blanket like deposition (minimal thickness variation) observed in the platform area (Fig. 6b). However, a moderate increase in thickness is found in the down-thrown block of the Vette fault near well 31/6-6, where a depocenter is also evident in the Draupne thickness map (Fig. 6a).

4.2. Mineral composition and texture

Bulk mineralogical analysis tells us the total percentage of minerals without indicating their origin. However, mineralogical information (i.e., the fraction of stiff and soft minerals) defines the geomechanical properties of the caprock. The bulk mineral fractions of Draupne and Heather formations are divided into three clusters; i) stiff quartz, feldspar, and pyrite (QFP), ii) soft clay and TOC, and iii) carbonate (Fig. 7). In general, the carbonate fractions within the study area are relatively low (<10%) except in the case of Heather Formation in well 32/4–1, which has 25% of carbonate (mainly siderite). The higher percentage of stiffer minerals (~70%) are found in the Draupne sample in well 35/11–4, while other samples have a higher percentage of softer minerals (>55%). The highest and lowest percentage of soft minerals are present in wells 32/2–1 and 35/11–4 in Draupne Formation, respectively. Individual quartz and clay fractions also show significant variations within the studied samples (Table 4). There is no significant variation observed between Draupne and Heather formations. However, within the same well higher percentage of stiff minerals are found in Heather Formation compared to the Draupne Formation.

Bulk mineralogy can be estimated from XRD analysis, but it is not possible to distinguish between the diagenetic or detrital phases. Therefore, petrographic observation is carried out to define the origin and texture of these constituents. Textural heterogeneity within the seal rocks is related to the relative alignment of minerals, mineral aggregates, organic matter or other components, and diagenesis, etc. Texturally caprock shales are often heterogeneous at the micrometer to millimeter scale when examined petrographically. In this study, scanning electron microscope (SEM) images from Draupne and Heather formations are analyzed to evaluate textural variation (Figs. 8 and 9). Draupne Formation in wells 32/2–1 and 32/4–1 is fine-grained with a matrix-supported framework compared to well 35/11–4, which has comparatively coarser grains with a mixed type framework. Both forms of shallow diagenetic pyrite (framboids and euhedral shape) are precipitated in well 35/11–4 (~22%), while wells 32/2–1 and 32/4–1 (1–2%) have only local framboid pyrite. Pyrite precipitation mainly depends on the initial pore fluids geochemical composition, where the pyrite framboids iron monosulfide (spherical aggregates of micrometer-sized pyrite crystals) is associated with organic matter (Figs. 8 and 9)

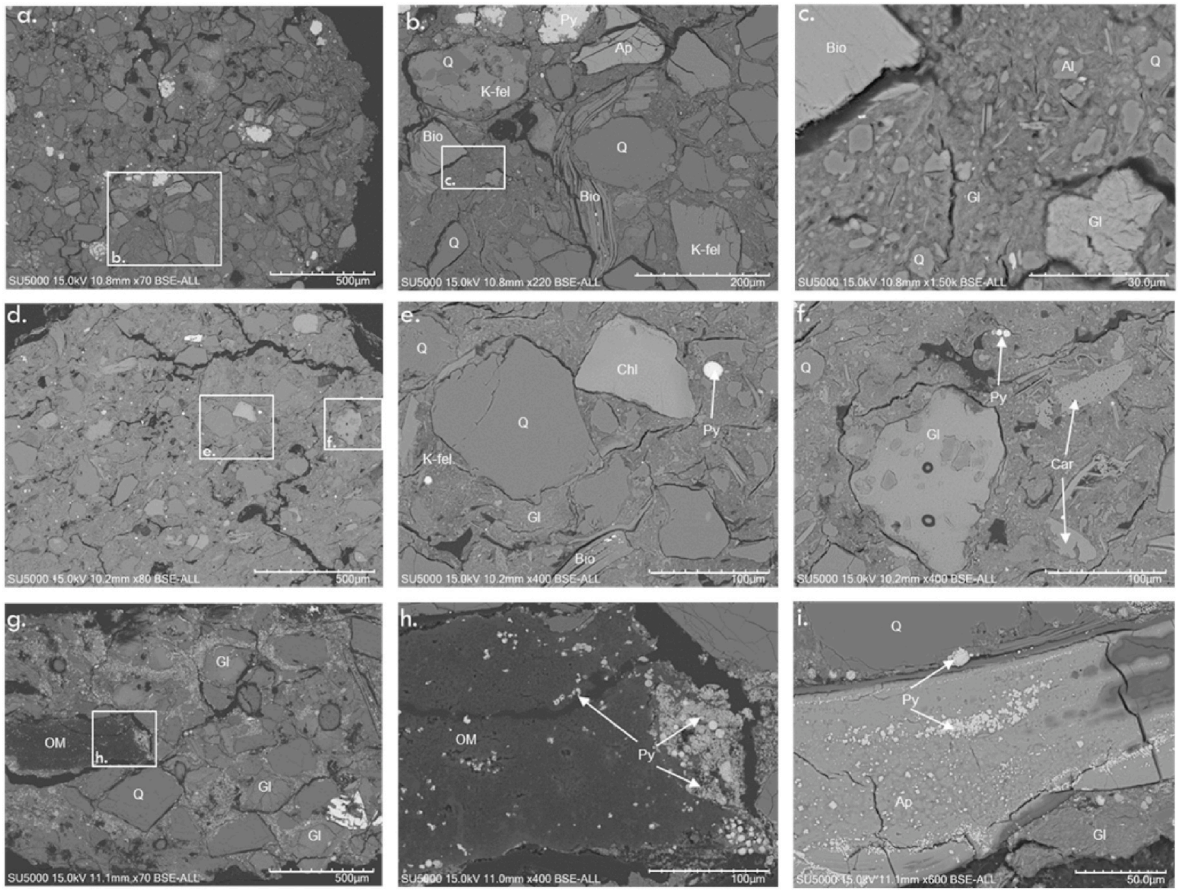

Fig. 8. High-resolution backscatter SEM images of Draupne Formation show the changes in composition and texture in a single caprock unit from wells 32/2–1 (a, b & c), 32/4–1 (d, e & f) and 35/11–4 (g, h & i). All the white dots are the pyrite (Py.) framboids and euhedral shape, which have a significant variation in volume and distribution within the studied wells. The abbreviations of Q.-Quartz, Gl.-Glauconite, Ap.-Apatite, Bio.-Biotite, K-fel.-K-Feldspar, Al.-Albite, Chl.-Chlorite, and Car.-Carbonate are used for simplicity. Note the variability of scale in different images.

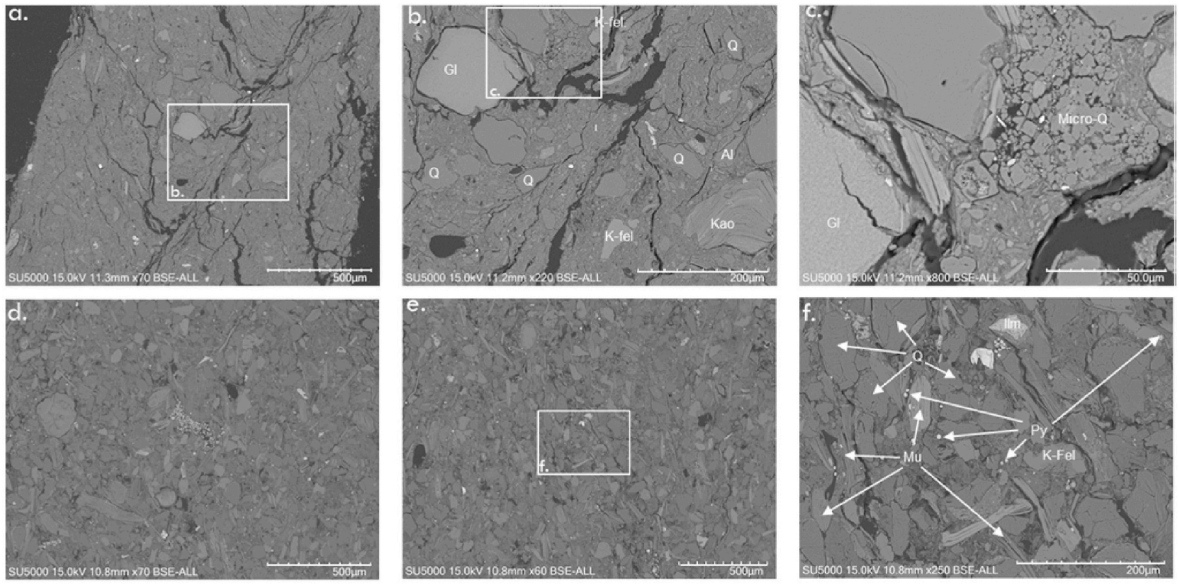

Fig. 9. High-resolution backscatter SEM images of Heather Formation show the changes in composition and texture from wells 32/2–1 (a, b & c) and 32/4–1 (d, e & f). The abbreviations of Q.-Quartz, Gl.-Glauconite, Kao.-Kaolinite, Mu.-Muscovite, K-fel.-K-Feldspar, Al.-Albite, Py.-Pyrite, and Ilm.-Ilmenite are used for simplicity. Note the variability in scale between images.

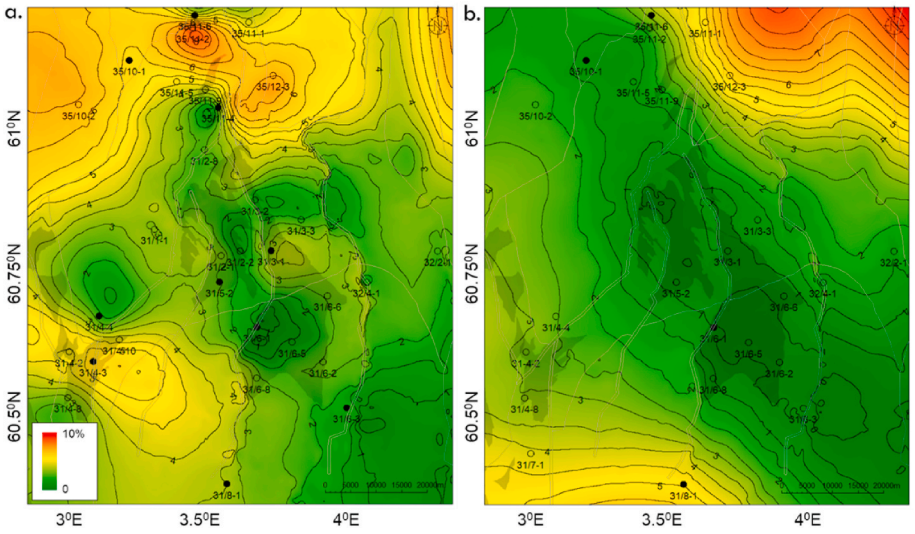

Fig. 10. Maps of TOC distribution based on the log derived well data points (harmonic average) of a) Draupne and b) Heather formations. Note that the contour interval is 0.5%.

and direct precipitation of micrometer-sized euhedral crystals are linked with iron oxide minerals (Fig. 8i) (Taylor and Macquaker, 2011). These observations indicate that there is a variation of initial fluid geochemical components between NW and SE wells. In contrast, Heather Formation has diagenetic quartz in both wells 32/2–1 and 32/4–1. Heather Formation has comparatively coarser grains compared to the Draupne Formation within the same wells except well 35/11–4, where a coarser Draupne Formation is observed. The number of samples is limited, but still, it is possible to identify the sub-zones with varying mineralogy and fabric. Based on our analysis, the NW part of the zero thickness trend is course-grained with low percentage of soft minerals assemblages compare to the south-eastern area where caprocks are fine-grained with a high percentage of soft minerals.

4.3. TOC distribution

Paleo-depositional variations also influence the variation in original TOC content and its preservation during and after deposition. The present-day TOC fraction depends on the anoxic condition of the seafloor during deposition and the preservation processes after deposition. The TOC distribution map based on well data points (calculated using equation (1)) shows significant TOC variation within the study area. Though there is considerable uncertainty in the calculated TOC (equation (1)), the harmonic average (Table 2) and the location of the measured TOC wells (solid black points in Fig. 10) added confidence in the TOC distribution map. Different TOC trends are observed between the Draupne and Heather formations. Lower TOC in Draupne Formation is found in the Troll area, which continued in the SE direction covering the Bjørgvin Arch and Stord Basin (Horda Platform), while the North and

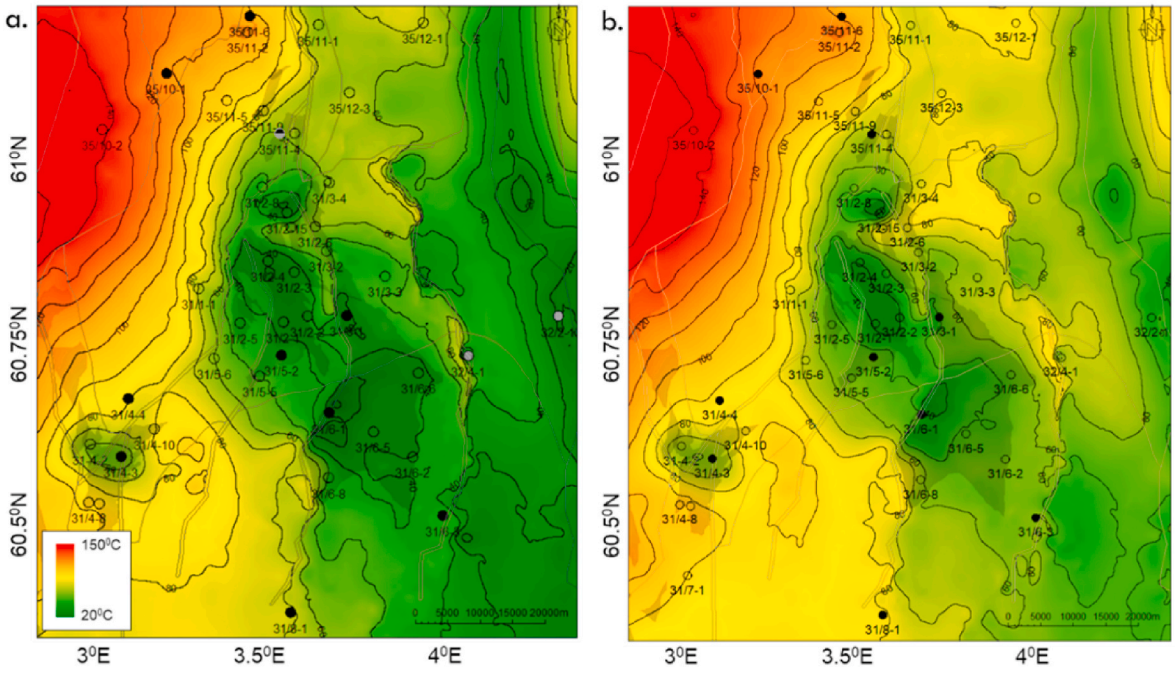

Fig. 11. The temperature map on top of Draupne Formation calculated using a geothermal gradient of 35 °C/Km representing a) present-day temperature and b) the maximum (exhumation corrected) temperature. The contour interval is 10 °C showing a gradual increase in temperature from southeast to northwest.

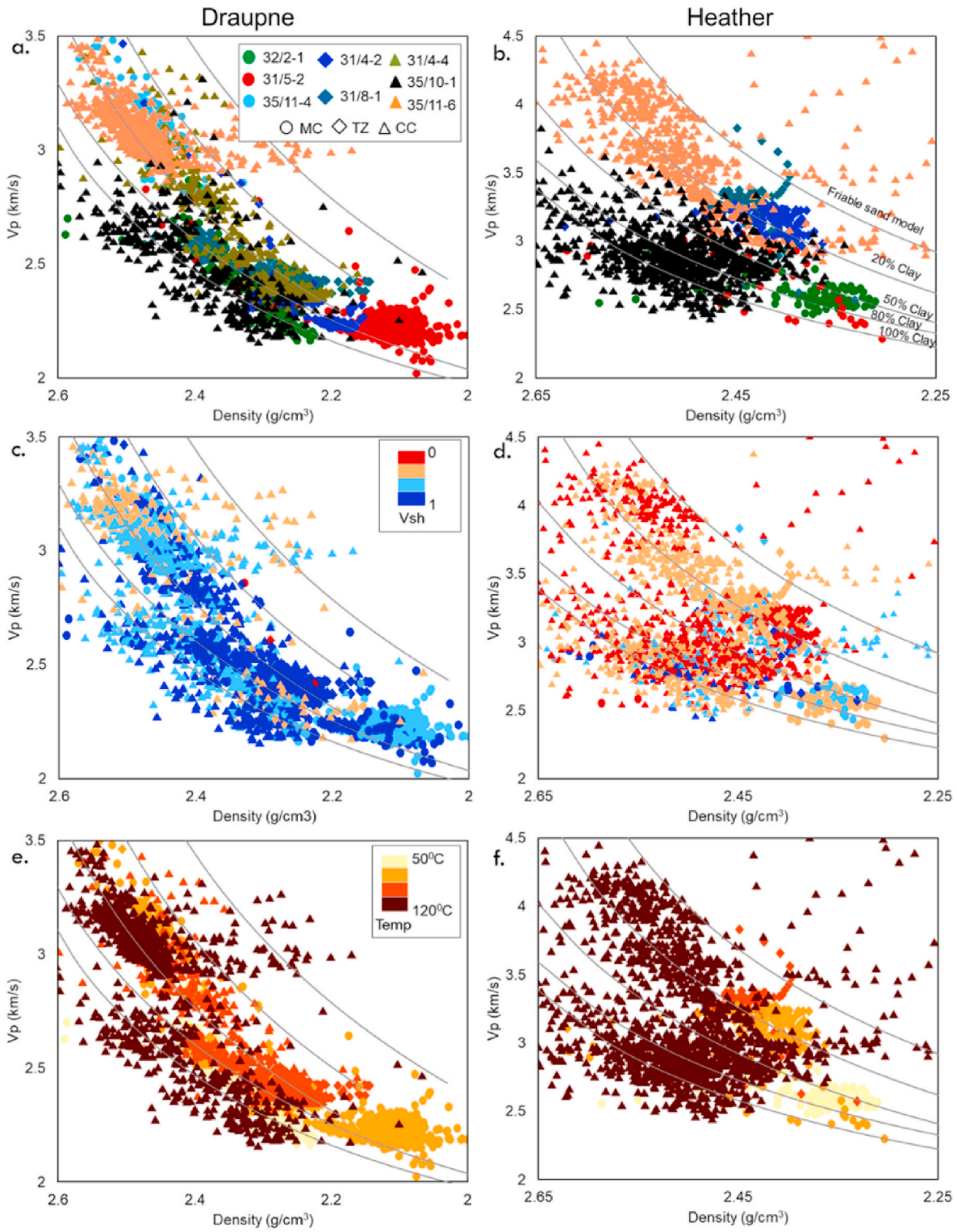

Fig. 12. Crossplots of Density versus Vp of Draupne and Heather formations from the eight selected wells representing MC, TZ, and CC data, color-coded by well names (a & b), Vsh (c & D) and Temperature (e & f) with the reference curves adapted from Avseth et al. (2005). (For interpretation of the references to color in this figure legend, the reader is referred to the Web version of this article.)

SW part of the areas have higher TOC covering the northern part of Lomre Terrace, Marflo Spur, and Brage Host. In contrast, Lower TOC in Heather Formation follows an NW-SE trend in the middle of the study area and increases both NE and SW directions (Fig. 10).

4.4. Compaction and properties of caprocks

The caprock properties are gradually altered due to the compaction processes (MC and CC). The transition between MC and CC in caprocks are mainly dependent on temperature and the mineralogy of the zone. Due to the lack of mineralogical analysis, the transition zone (TZ) of the

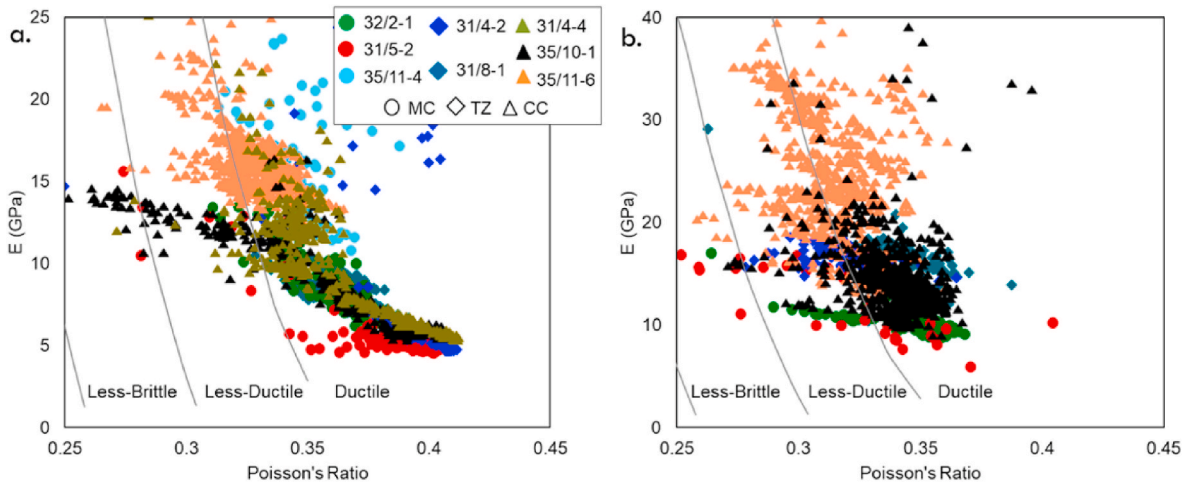

Fig. 13. Cross-plot of Young's modulus versus Poisson's ratio of a) Draupne and b) Heather formations with the reference curves adapted from Perez and Marfurt (2014).

studied area is defined by only the maximum temperature experienced by the caprock formations. The mechanical compaction in sandstone is dominated at temperature 70 °C considering 35 °C/km geothermal gradient; however, the transition for fine-grain particle-like shale depends on many other factors (i.e., mineralogy, type of clay, pore water chemistry, etc.) and ranges between 60^0 to 120 °C (Bjørlykke et al.,

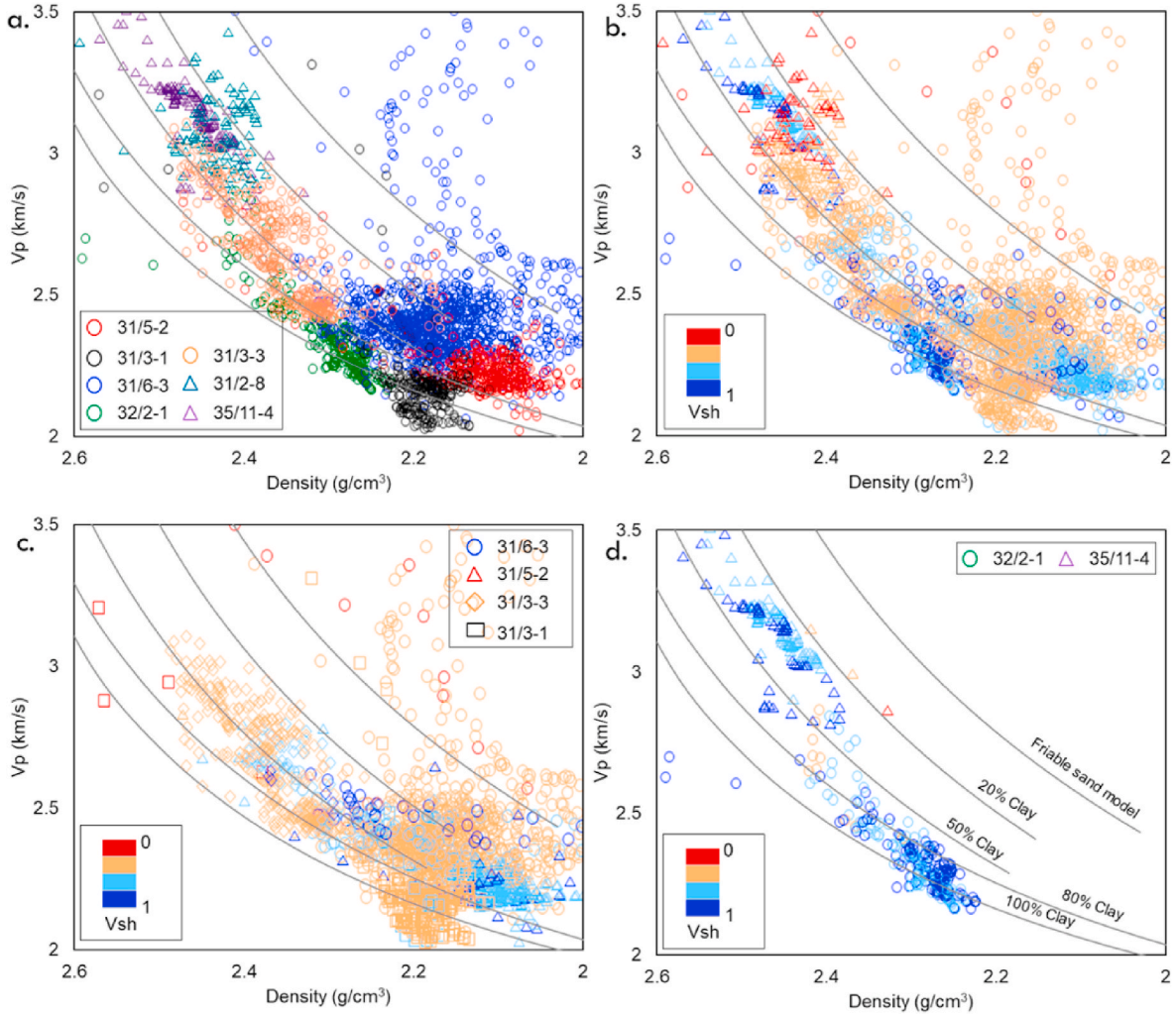

Fig. 14. Crossplots of density versus Vp of Draupne Formation data from the mechanically compacted (MC) wells color-coded by well names (a), and Vsh (b, c & d) with the reference curves adapted from Avseth et al. (2005). The circle represents the wells located in the SE part from zero thickness, while the triangles represent the NW wells. (For interpretation of the references to color in this figure legend, the reader is referred to the Web version of this article.)

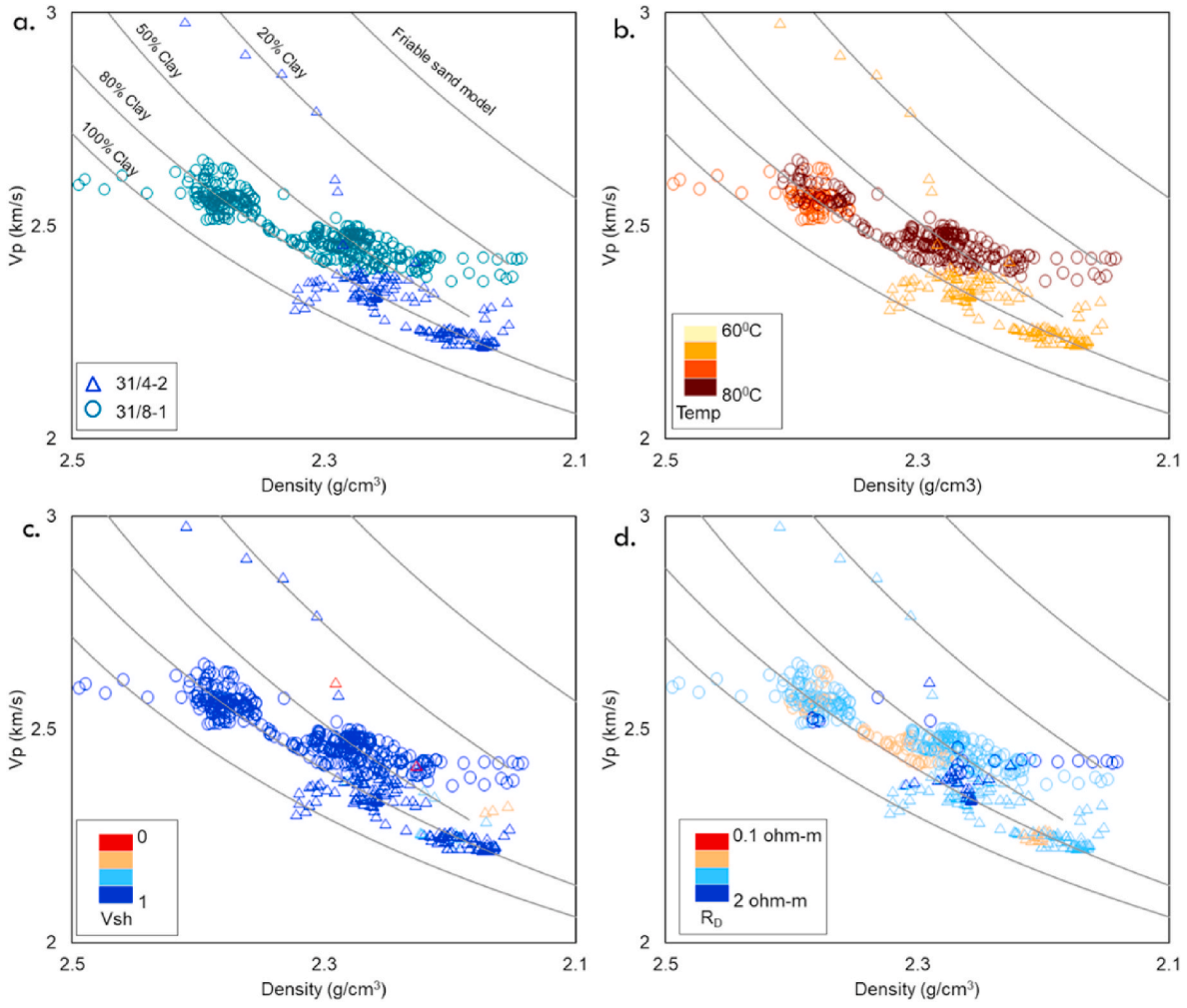

Fig. 15. Density versus Vp cross-plot of Draupne Formation based on data from the transition zone (TZ) wells color-coded by well names (a), temperature (b), Vsh (c), and R_D (d) with the reference curves adapted from Avseth et al. (2005). (For interpretation of the references to color in this figure legend, the reader is referred to the Web version of this article.)

2015). In this study, a range, i.e., 65–75 °C is used as a transition zone considering the uncertainties. According to present-day temperature on top of the Draupne Formation, the majority of the studied wells are within the MC zone compared to TZ and CC. However, after the exhumation correction, the numbers of wells falling in TZ and CC are increased (Table 3). The present and maximum temperature map on top of the Draupne Formation show the spatial distribution within the different sub-groups (Fig. 11). The northwestern part of the studied area is in the realm of chemical compaction, which covered the Lomre terrace and Marflo Spur structural elements. In contrast, the western part of the Stord Basin is within the TZ temperature, and the rest of the platform, including the Troll Gas Field area, is within the MC zone. A similar temperature trend is also observed in the Heather Formation temperature distribution maps.

The Vp and density data of Draupne and Heather formations from eight wells covering all sub-groups (MC, TZ & CC wells) are cross-plotted to evaluate variations of the caprock elastic properties (Fig. 12). We find no specific clusters for different sub-group in Draupne Formation; instead, a mixture of different well clusters is observed. The stiff rock (high Vp & density) data points are from an MC well 35/11–4 and a CC well 35/11–6, while the soft rock (low values of Vp & density) is represented by an MC well 31/5–2 and the TZ well 31/4–2. The rest of the wells, which are from all three sub-groups, show data in the intermediate range. We find no trend in Vsh and temperature as high and low-temperature data is clustered in the same region (Fig. 12e). Heather Formation also shows a similar pattern (no sub-group clustering) of data distribution and temperature variation, but overall the elastic properties have higher values compare to Draupne Formation (Fig. 12b). Moreover, in this formation, all the wells show silty to sandy type shales, which have significant variations of elastic properties compared to the Draupne data points.

Geomechanical properties in the study area show similar trends like acoustic properties. The wells plotted in the Vp-density plain also used in this analysis, which covers wells from MC, TZ, and CC zones. The soft Draupne Formation (low E and high PR) data points are plotted from wells 31/5–2, 31/4–2, 32/2–1, and 31/8–1 while high values of E and comparatively low values of PR observed in wells 35/11–4 and 35/11–6 (Fig. 13). However, the data from wells 31/4-4 and 35/10-1 have a wide-range where data from both wells started in the very soft-clustered area but ended up following the trend with a significant decrease in PR. A gentle increase in E is found in well 35/10–1, and an increase in E with a constant PR observed in well 31/4-4 (Fig. 13a). In contrast, Heather Formation seems to be stiffer than Draupne Formation but follows a similar increasing trend (i.e., increasing E but with a constant range of PR) (Fig. 13b). For further analyses, individual sub-groups are investigated in the successive sections under the different subheadings.

4.4.1. Caprock properties in shallow depth wells (MC)

Vp and density data points of seven wells of Draupne Formation located in the MC zone (MCZ) are chosen to evaluate variations of

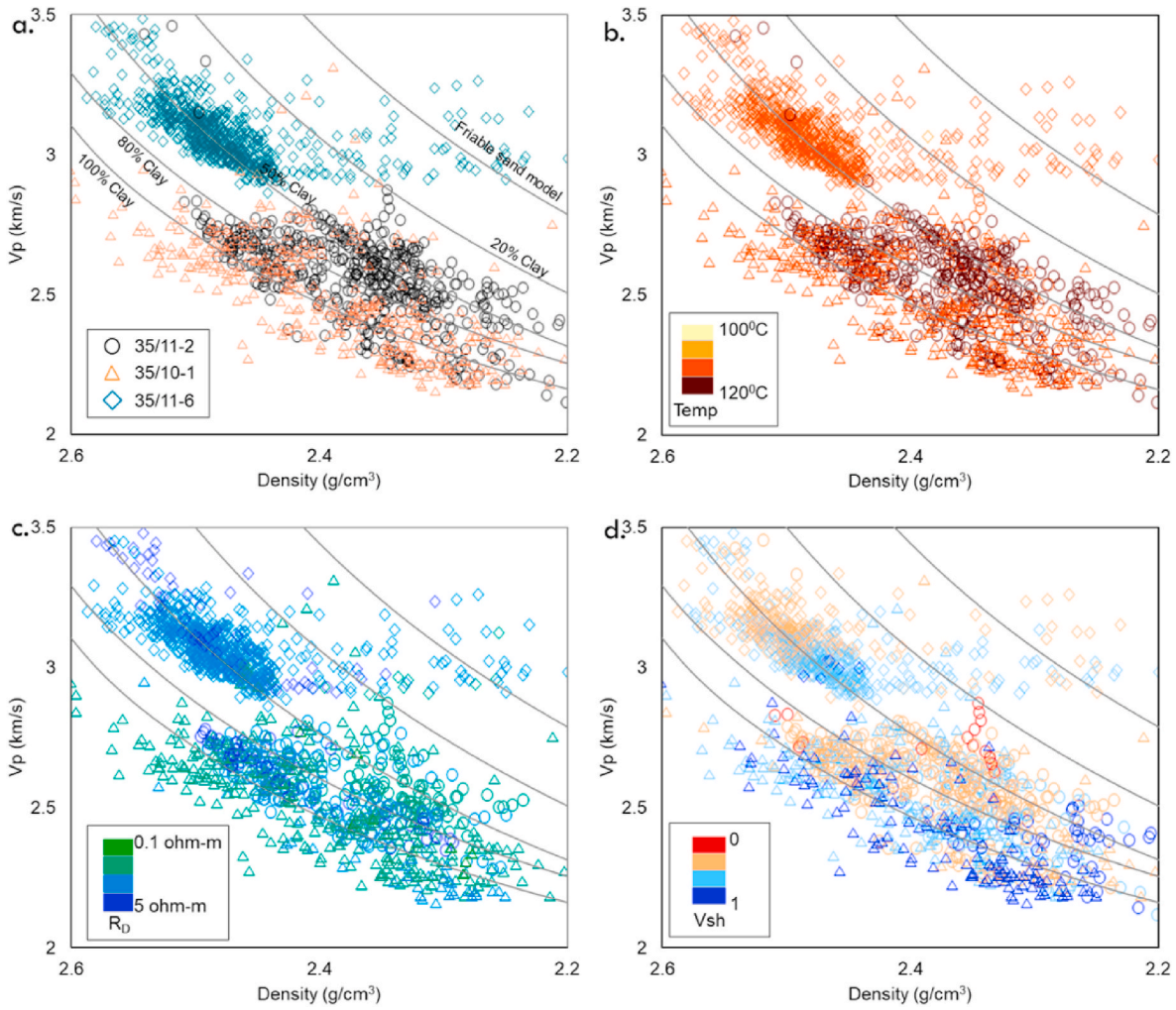

Fig. 16. Cross-plot of density versus Vp of Draupne Formation data retrieved from the chemically compacted zone (CCZ) color-coded by well names (a), temperature (b), deep resistivity (c), and Vsh (d) with the reference curves adapted from Avseth et al. (2005). (For interpretation of the references to color in this figure legend, the reader is referred to the Web version of this article.)

caprock properties. Two different symbols (i.e., circles and triangles) are used to separate the NW, and SE wells, where the circles represent SE, whereas the NW wells are denoted as triangles. The Draupne Formation situated in MCZ shows a significant variation of Vp and density where the NW wells 31/2–8, and 35/11-4 show stiff nature (high Vp & Density) compared to the wells from the SE part (Fig. 14). However, the well 31/3-3, which is located in the SE part, has an intermediate range of properties. Vsh values within the studied MC wells also vary significantly. Wells 31/5–2, 32/2–1, and 35/11–4 are more clayey compared to the other wells, whereas wells 31/3–1, 31/3-3, and 31/6–1 are less clayey with almost 0% clay in well 31/2–8. However, the distribution of caprock properties within the wells is not following the mechanical compaction trend. For example, wells 31/2–8 and 35/11-4 have a significant variation in Vsh but cluster in one location, while wells 31/3–1, 31/5–2, 31/6–1, and 32/2–1 contain soft rock with different depth and Vsh value. Another observation between wells 32/2–1 and 35/11–4 is that both wells have a high percentage of Vsh where well 32/2–1 follows the higher clay reference curve (80–100% clay line), while well 35/11–4 is shifted diagenetically and follows the 50-20% clay curves (Fig. 14d). The high values of Vp and density in well 35/11-4 might be due to a difference in grain size and precipitation of pyrite (Fig. 8h&i). Therefore, the higher Vsh percentage has not much effect on density and velocity in this case. On the contrary, the Draupne zone is silty in well 21/2–8 owing to a low Vsh value with high values of Vp and density. Therefore, the log driven caprock properties need validation with the petrographic analysis before deriving any conclusion.

4.4.2. *Caprock properties in intermediate depth wells (TZ)*

Two wells penetrated the studied caprocks in TZ are analyzed for characterizing the caprock properties. Data points from wells 31/4–2 and 31/8-1 have lower Vp and density values. All the wells have a high percentage of clay content (high Vsh) generally following the 80% clay curve. However, data from wells 31/8–1 and 31/4–2 are scattered within the 80-50% clay range. Overall the data signify the soft nature of the caprock zone though the temperature is quite high (Fig. 15b).

4.4.3. *Caprock properties in deeply buried wells (CC)*

Draupne Formation falling in the CC zone (CCZ) in three wells within the study area is plotted in the Vp-density rock physics template to evaluate variations of rock properties within the CC wells (Fig. 16). There are significant variations of rock properties observed where well 35/11-6 has stiff (high Vp & density) rocks compared to wells 35/10–1 and 35/11–2. Though the difference in temperature and resistivity values are not significant, comparatively lower temperatures and higher deep resistivity are found in well 35/11–6. The Vsh values show considerable variations within the wells and with the reference curves. The soft (low Vp and density) properties well 35/10-1 has high values of Vsh and follow the 100% clay line. However, the data points of well 35/11-2 shift upward, having higher values of velocity and similar density with decreasing Vsh. In contrast, well 35/11-6 has higher Vp and density

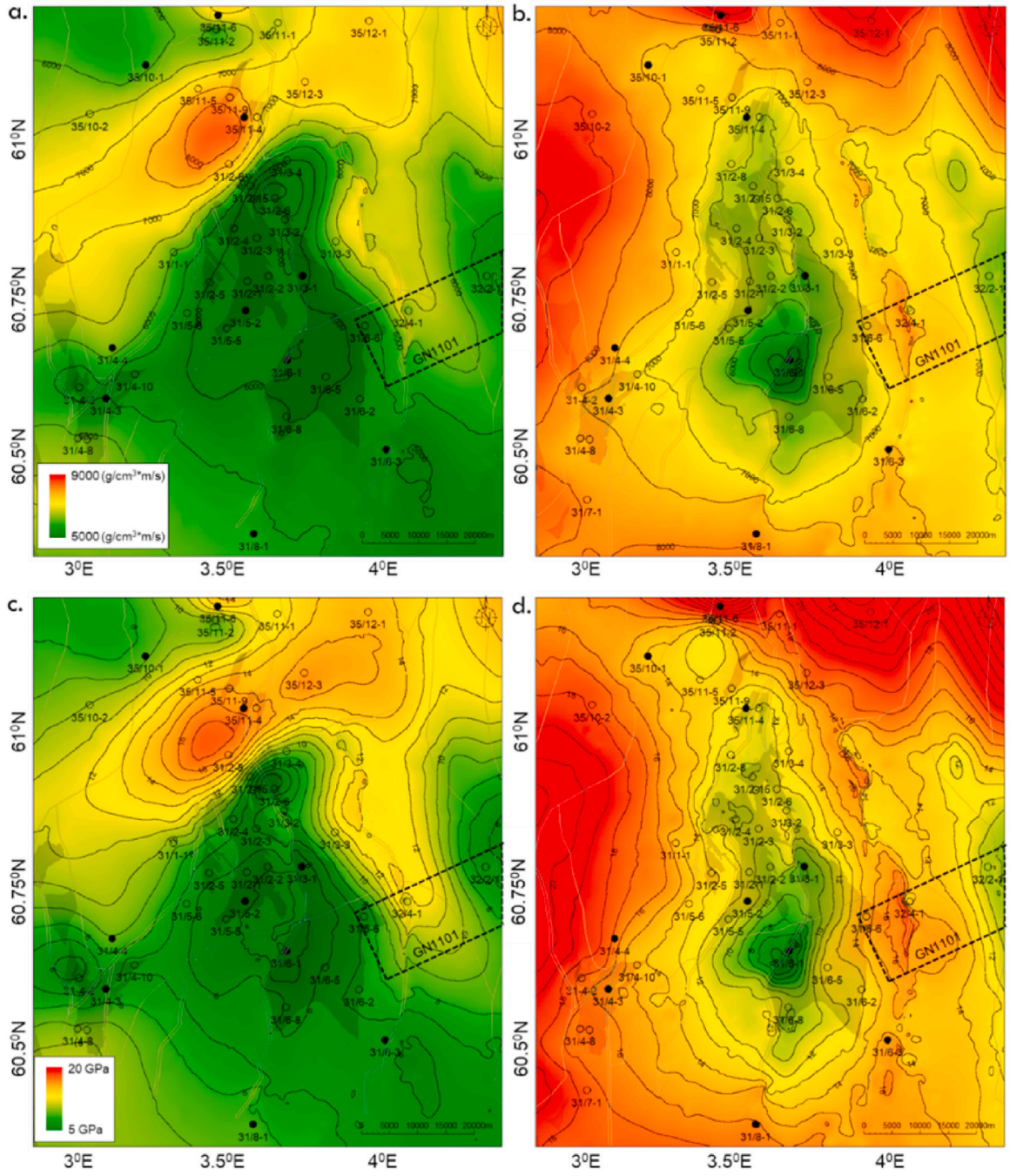

Fig. 17. Caprock property maps generated using the well data points of Draupne and Heather formations showing AI in Draupne (a), AI in Heather (b), E in Draupne (c), and E in Heather (d). The same color scale is used for each property within both formations to show the variability. (For interpretation of the references to color in this figure legend, the reader is referred to the Web version of this article.)

but the same range of Vsh compared to well 35/11–2 (Fig. 16d).

Differences in caprock properties within the studied wells also reflected in the property maps generated from the average values. Acoustic Impedance (AI) and Young's Modulus (E) of Draupne and Heather formations' spatial distribution within the studied area are shown in Fig. 17. The same color scale is used for both formations to compare those properties variations visually. Both formations have lateral change within the study area where the Draupne Formation has higher contrast than the Heather Formation. Moreover, the property variation tends to follow the structural elements, especially the major faults. The softer Draupne caprock (low values of AI and E) found in the Troll area is bounded by Vette fault in the east and Troll fault in the west. There is a stiff rock trend observed in the north of the Troll field, which follows a NE-SW strip. However, following the stiff rock trend, a comparatively softer rock found in the north-western corner of the study area. In contrast, Heather Formation's rock properties follow a different pattern where the relatively soft rock is found in the Troll Field area, which gradually becomes stiff in all directions.

4.5. Brittleness indices

Draupne and Heather formation's brittleness indices values are summaries in Table 5. Four different BI's (EBI^1, EBI^2, MBI^1 & MBI^2) are estimated to evaluate the geomechanical properties of the caprocks

Table 5
Comparison of average brittleness indices within various structural elements, and brittleness calculated by different equations for Draupne and Heather formations.

Well no.	Structural Elements (NPD)	Draupne Formation				Heather Formation			
		EBI1	EBI2	MBI1	MBI2	EBI1	EBI2	MBI1	MBI2
31/2-1	Bjørgvin Arch	0.14	0.18	–	–	–	–	–	–
31/2-2		0.13	0.07	–	–	–	–	–	–
31/2-6		0.17	0.02	–	–	–	–	–	–
31/2-8		0.36	0.50	–	–	–	–	–	–
31/3-1		0.14	0.17	–	–	0.22	0.38	–	–
31/3-2		0.24	0.15	–	–			–	–
31/3-3		0.25	0.31	–	–	0.29	0.39	–	–
31/4-3		0.18	0.23	–	–	–	–	–	–
31/4-8		0.21	0.33	–	–	–	–	–	–
31/4-10		0.16	0.20	–	–	–	–	–	–
31/5-2		0.13	0.17	–	–	0.27	0.42	–	–
32/2-1		0.14	0.26	0.19	0.27	0.23	0.37	0.27	0.43
35/11-7		0.34	0.49	–	–	–	–	–	–
31/6-1	Stord Baisn	0.13	0.17	–	–	0.17	0.26	–	–
31/6-2		0.18	0.24	–	–	0.30	0.41	–	–
31/6-3		0.15	0.24	–	–	0.33	0.48	–	–
31/6-5		0.14	0.14	–	–	0.28	0.41	–	–
31/6-6		0.17	0.22	–	–	0.32	0.46	–	–
31/6-8		0.14	0.20	–	–	0.23	0.36	–	–
31/8-1		0.18	0.28	–	–	0.34	0.50	–	–
32/4-1		0.26	0.36	0.26	0.31	0.28	0.43	0.17	0.49
31/4-4	Lomre Terrace	0.19	0.32	–	–	–	–	–	–
35/11-2		0.21	0.37	–	–	0.36	0.55	–	–
35/11-4		0.32	0.49	0.61	0.70	–	–	–	–
35/11-6		0.28	0.41	–	–	0.53	0.61	–	–
31-4-2	Brage Host	0.13	0.23	–	–	0.38	0.51	–	–
35/10-1	Marflo Spur	0.20	0.31	–	–	0.29	0.46	–	–

where the EBI's are calculated using elastic properties, and mineralogical fractions are used to estimate the MBI's. Overall the Draupne and Heather formations show the BI values tend to be more ductile with few less ductile readings in Heather Formation. However, there is a significant variation observed within the values estimated by the various BIs. $EBI^{1,}$ which is calculated from Young Modulus (E) and Poisson's ratio (PR), has lower BI values than $EBI^{2,}$ which is estimated using AI and R_D. Similar differences are also found between MBI^1 and MBI^2 where MBI^2 has higher BI value than MBI^1. This is expected as MBI^2 considered all the brittle minerals (i.e., quartz, feldspar, pyrite, and carbonate) to calculate BI compared to only quartz in MBI^1. However, EBI^1 has a good match with MBI^1 and, similarly, EBI^2 with MBI^2. In well 35/11–4, where the percentage of ductile minerals (Clay and TOC) has a meager influence, the estimated MBIs are significantly higher than EBIs. Moreover, this well represents the highest BI value (0.70) within the studied wells.

BI maps of Draupne and Heather formations show a significant lateral variation of the caprock brittleness properties within the study area (Fig. 18). According to the maps, the less ductile zones are found in Heather Formation, which is calculated using equation (8) (Fig. 18d). Overall, as seen in the well average, EBI^2 is stiffer than $EBI^{1,}$ wherein both scenarios, Heather Formation is less ductile, the BI maps also represent a similar trend. Moreover, the maps illustrated that the more ductile caprock located in the center of the study area, mainly covering the Troll Field and gradually increasing in all directions. However, in Draupne Formation, a NE-SW trending brittleness anomaly exists in the NW corner of the study area (Fig. 18a&c).

4.6. Brittleness indices trend

In this analysis, we are evaluating the qualitative brittleness increasing trends based on elastic impedance-based brittleness in Young's modulus (E) versus Poisson's ratio (PR) and LMR (LamdaRho versus MuRho) templates. We choose six wells (31/4–2, 31/8–1, 32/2–1, 35/10–1, 35/11–4 & 35/11–6) with different depth levels to cover the whole vertical compaction ranges and cover the area spatially. There is a significant difference observed in brittleness increment trend when compared with reference curves (Figs. 19 and 20). According to Grieser and Bray (2007) zonation, the studied Draupne and Heather formations data points fall within the brittle area though the brittleness indices values are quite low (Fig. 19). However, the brittleness indices increase with increasing E.

There is also a significant difference observed in the brittleness increment trend between the studied data points and reference curves in the E versus Poisson's ratio cross-plots (Fig. 20). In E versus PR cross-plot, the Draupne and Heather formations data points follow an increased brittleness trend with increasing E and a constant range of PR. Moreover, a zone of very low values of E and high values of PR is found, which does not follow the trend and exhibits very low brittleness hence deemed ductile. Similar different pattern finds in $\lambda\rho$ versus $\mu\rho$ cross-plots where the reference curve brittleness increases with a moderate rise in $\mu\rho$ and decrease in $\lambda\rho$ while brittleness of Draupne and Heather formations increase with increasing $\lambda\rho$ and $\mu\rho$ (Fig. 20c & d).

4.7. Variation of AI in prestack inverted cube

The prestack inverted cube of acoustic impedance (AI) of Draupne and Sognefjord formations shows the lateral amplitude variation in the Smeaheia area (Fig. 21b). An increasing trend of amplitude follows the time structural dipping trend, i.e., increases from NE to SW direction (Fig. 21a). A similar amplitude increasing trend also observed in the cross-section where the AI value of Draupne and Heather formations gradually increases from NE to SW direction (Fig. 21c), which strongly follows the log-derived elastic and geomechanical properties (Fig. 17). The log-based AI and Young's modulus (E) of Draupne and Heather formations within the seismic cube boundary (GN1101) show a similar gradual increase in properties. Moreover, the elastic log-based brittleness indices estimated using empirical equations confirm the same trend (Fig. 18). The relation between inverted seismic volume and geomechanical property (i.e., brittleness) helps for the qualitative characterization of organic-rich caprock from seismic data.

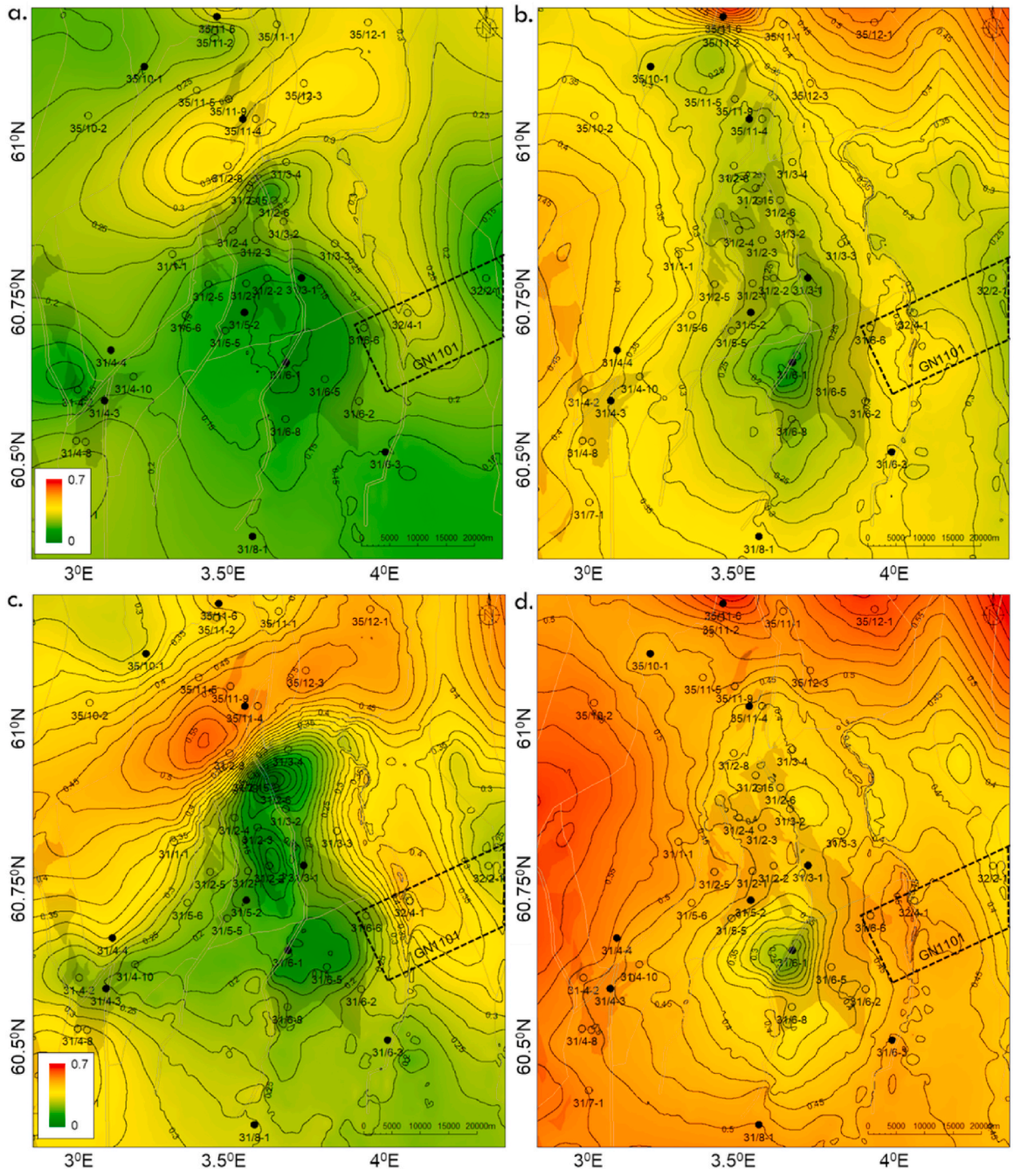

Fig. 18. Brittleness Index maps calculated from average well data points using Grieser and Bray (2009) for a) Draupne and b) Heather formations, and Fawad and Mondol (2020, unpublished, patent-pending on the procedure) for both c) Draupne and d) Heather formations. The contour interval is 0.025, and the same color scale is used for all the maps to show the variability between equations and formations. (For interpretation of the references to color in this figure legend, the reader is referred to the Web version of this article.)

5. Discussion

5.1. Paleo depositional environment

Based on the gamma-ray log pattern, height, and the corresponding values (Emery and Myers, 1996), a significant variation is found in the paleo-depositional environment of Draupne and Heather formations within the study area. This differences might influence the mineralogy, grain size, fabric, initial pore fluids geochemistry, etc. as shales in a basin typically follow a systematic vertical pattern with the fluctuation of relative sea-level changes. However, tectonics, climate, and relative sea-level condition affect the ultimate character of that basin-fill succession (Slatt, 2011). These factors have a direct effect on the caprock integrity, which are observed in log derived elastic and geomechanical properties. However, without a basin-wide analysis of the sediment input and deposition system, it is challenging to identify the factors that influence a small area like this study. Considering these uncertainties, gamma-ray still represents the local variation and proves to be an excellent tool for qualitative interpretation.

According to the gamma-ray log shape and value in the studied area, the possible high energy sediments (mainly silt) within Draupne caprock was deposited in the NW close to the Lomre Terrace area, while in the SE (including the Bjørgvin Arch, and Stord Basin) possessed a proximal shelf depositional environment within a marine embayment. However,

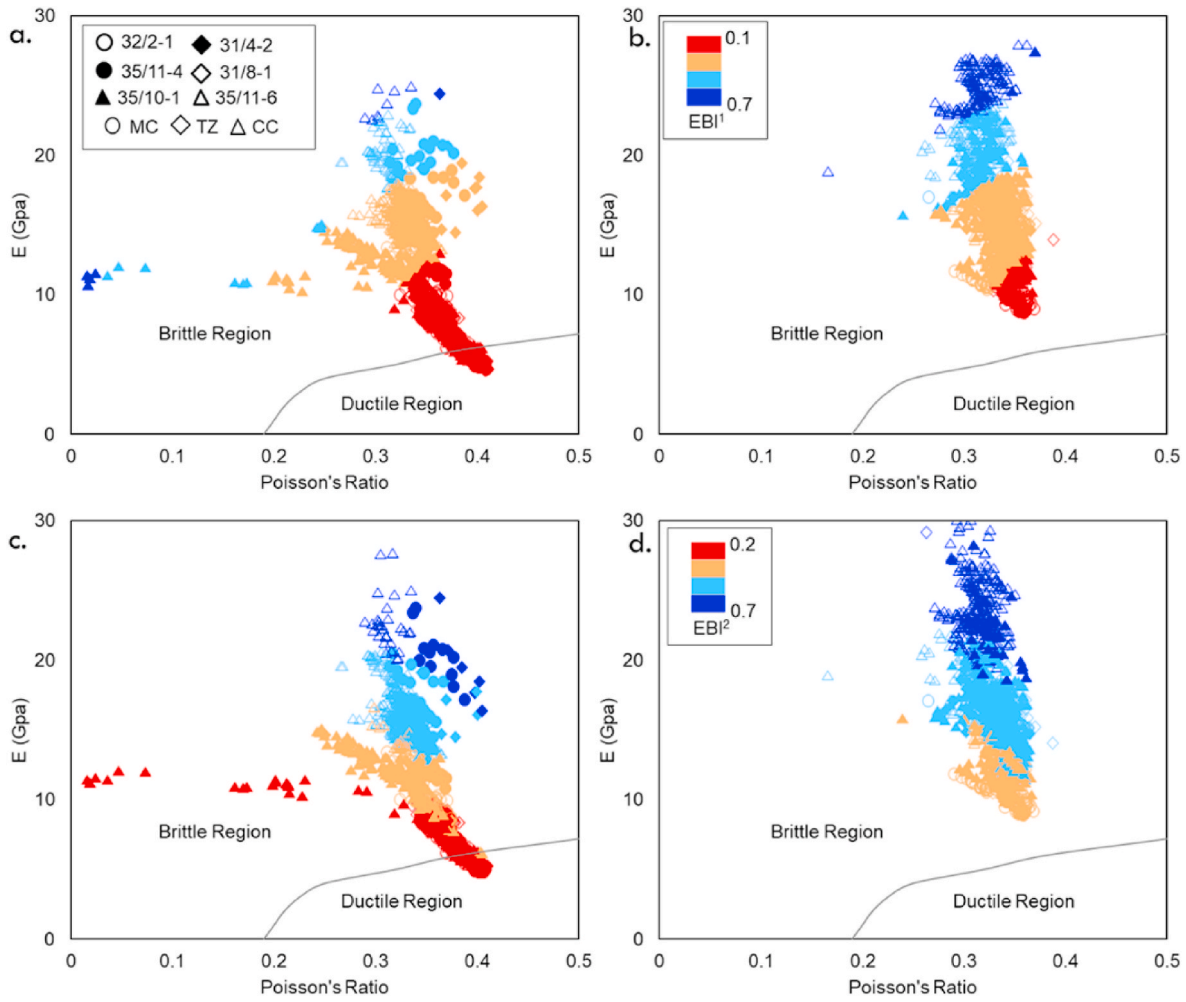

Fig. 19. Young's modulus versus Poisson's ratio cross-plots of Draupne (a) and Heather (b) formations color-coded by EBI^1 and same formations in (c) and (d) color-coded by EBI^2 with the reference curve adapted from Grieser and Bray (2007).

the distal shelf environment in the SW and western areas, which cover the SW part of the Stord Basin and Lomre Terrace, is more clayey with a higher fraction of organic matter. Other major faults (i.e., Vette, Tusse, Svartalv, Idunn, etc.) also influenced the local thickness, which ultimately impacted the mineralogy, grain size and fabric, and initial pore water chemistry. The local depocentres interpreted in the thickness maps explain the effect of the fault-related accommodation spaces variation during deposition, and the consequence of that was also observed in the log shape and vertical stacking pattern differences within the studied wells (Fig. 5). These depositional variations influenced the mineral assemblages within Draupne and Heather formations. Significant changes of stiff (i.e., quartz, pyrite, feldspar, and carbonate) and soft (i.e., clay, organic matter) mineral fractions were found within NW (35/11–4) and SE (32/2–1 & 32/4–1) wells. The well 35/11-4 has courser grains with the abundance of pyrite and a small fraction of clay mineral while wells 32/2–1 and 32/4-1 have fine-grained (clay fractions) with local clustering of pyrite and a small fraction of quartz in Draupne Formation (Figs. 7–9). In Heather Formation, micro-quartz (32/2–1) and abundance of siderite (32/4–1) are found where the ratio of soft and stiff mineral assemblages are 50:50.

5.2. Effect of compaction

The Draupne Formation data point cluster does not separate mechanical and chemical compacted wells; instead, the data overlapped different regions (Figs. 12 and 13). Similar data distribution trends are also found in Heather Formation, but the properties have higher values and different trends compared to Draupne Formation. The wells located in high-energy deposition area (i.e., in the NW close to troll fault, i.e., 31/2–8, 35/11–4 & 35/11–6) have higher values of acoustic and geomechanical properties compared to the SE platform and SW deep basin areas (e.g., wells 31/4–2, 31/4-4, 31/5–2, 32/2–1 & 35/10–1). Grain size and sorting also have a significant impact on caprock properties. Larger grain size with mixed type of rock framework (a mix between matrix and grains) were observed in NW well (35/11–4) compared to the SE wells (32/2–1 & 32/4–1) where grains are finer making a matrix-supported caprock. The grain sizes and their distributions are other possibilities for stiffer zones in NW wells because poorly sorted coarse-grained sediments compacted more than the fine-grained shales (Storvoll et al., 2005; Mondol et al., 2007; Marcussen et al., 2009; Thyberg et al., 2009). Moreover, homogeneous fine-grained rocks can preserve higher stress; hence behave more ductile than heterogeneous coarse-grained rocks. Also, larger grain size makes rocks easier to fracture thus is stiffer (Zhang et al., 2016) because of more inter-granular cracks within small grains, which allow mobilizing more strength, also the larger grains containing larger and longer inter-granular cracks lower stress is required to initiate and propagate cracks (Eberhardt et al., 1999).

The sections of Draupne and Heather formations exposed to chemical compaction (i.e., 35/10–1, 35/11–2 & 35/11–6) also show a significant variation of caprock properties where the stiff data points (high Vp, high density, and high E) fall within the same range with sections that only

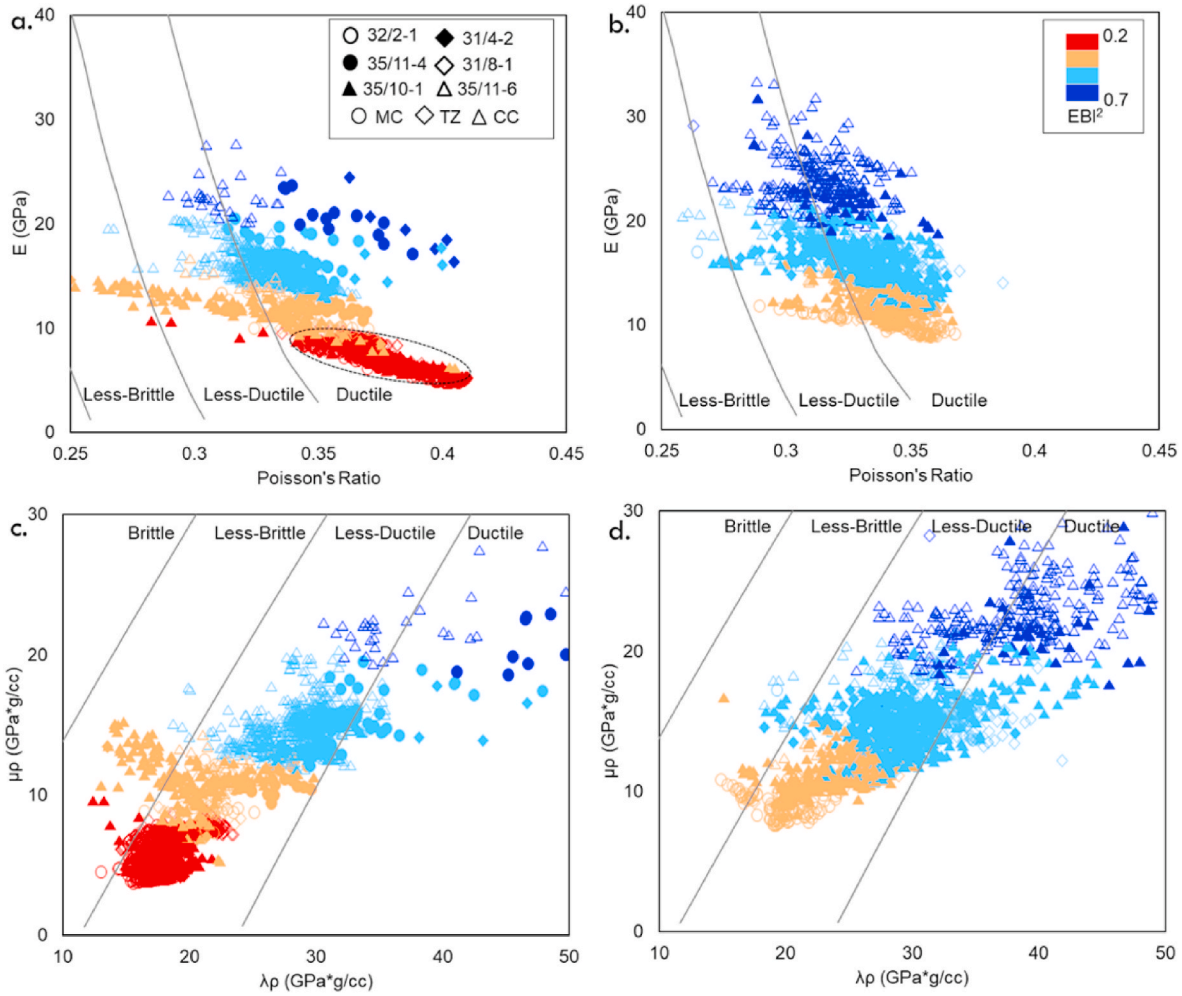

Fig. 20. Cross-plots of data points from six wells show the Young's modulus versus Poisson's ratio of Draupne (a) and Heather (b) formations and the μρ versus λρ of Draupne (c) and Heather (d) formations with the reference curves adapted from Perez and Marfurt. (2014). All the cross plots color-coded with EBI^2 brittleness indices value.

experienced mechanical compaction (i.e., wells 31/2–8, 21/3-3 & 35/11–4). The location of the well 35/10–1 is in the deep basin area, which explains the high Vsh percentage. Moreover, the wells 35/11–2 and 35/11-6 located in its close proximity also manifest a similar range of Vsh values. There might be an effective-stress difference in reservoir-caprock pair between dry hole (35/11–6) and discovery (35/10–1 and 35/11–2) wells as both reservoirs contain different fluids at different reservoir pressure. These might be leading to a different compaction process with variation in caprock properties. The effect of depth (equivalent temperature) on caprock properties might have acted in both ways (decreasing or increasing stiffness) because of the combined impact of pressure, temperature, diagenesis, and TOC as functions of depth. TOC itself has a complex effect on caprock properties. The maturation of TOC increases porosity hence increase rigidity (Rybacki et al., 2016) while during conversion, the heavy residual TOC portion increases the bulk density hence the rock stiffness. However, the effect of TOC on caprock geomechanical properties more depends on fabric (i.e., sparsely or layered distribution) than the TOC volume fraction (Slatt and Abousleiman, 2011). Moreover, in fine-grained, thick shale formations, there might be possibilities of developing overpressure by un-expelled fluid resulting in the reduction of the effective stress, hence decreasing the caprock stiffness. The low values of acoustic and geomechanical properties of chemically compacted wells (NW) within the study area might be the effect of those parameters (Fig. 4). The immature TOC in the SW part of the study area representing low values of elastic properties is possibly a function of weak mineral contents (i.e., clay and TOC), rather than a TOC alteration effect. This indicates the immature TOC behaves like a soft mineral assemblage.

5.3. Brittleness indices

In MBI^1, which is only considered quartz as stiff mineral, underestimated the formation of brittleness and has a poor correlation with caprock properties (Fig. 22a&e). However, considering the total stiff minerals, we found a better correlation compare with only quartz (Fig. 22c&e). Moreover, the mineralogy based brittleness indices are sometimes overestimating because the equations do not consider any diagenetic effects such as compaction related grain fabric or chemical precipitation (i.e., pyrite or quartz cement, etc.). The process does not consider the origin of the mineral assemblages (i.e., detrital or diagenetic), which has a significant impact on rock mechanical behavior too. For example, in well 35/11–4, the mineralogical BI's are significantly higher than the elastic property-based BI's because MBI's only considered bulk mineralogy fractions but did not consider the effective rock framework impact. On the other hand, the estimated elastic properties have embedded consideration of depositional and diagenetic effects, which is reflected in the EBI's assessed values (Table 5). Moreover, EBI's increasing trend is significantly different than the published trends (Figs. 19 and 20). The zones defined in the background curves are estimated from the data points of Barnett shale from the Fort Worth

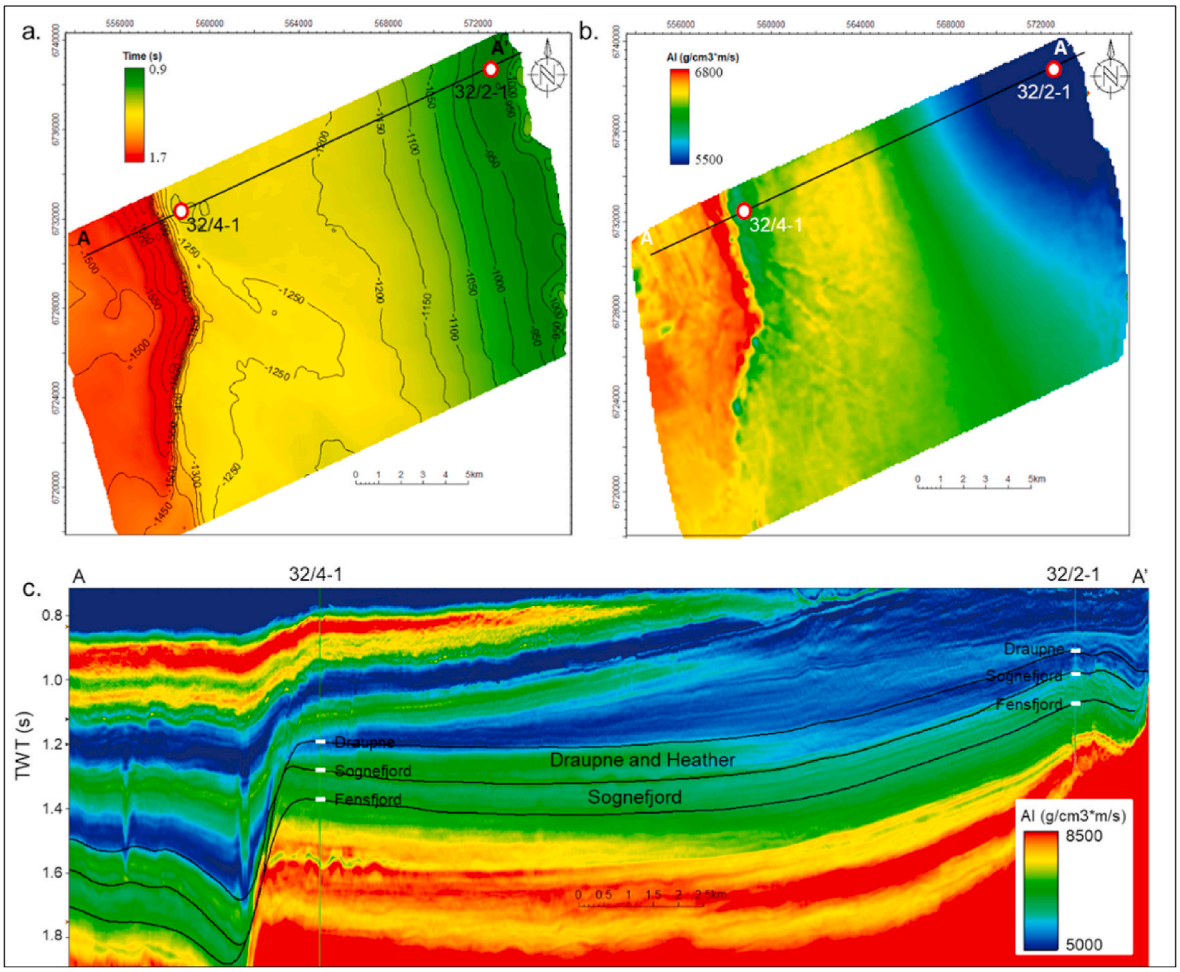

Fig. 21. a) Time structure map of Draupne Formation based on the 3D seismic data outlined in Fig. 1, with the location of random line A-A′ and exploration wells 32/2–1 and 32/4–1. B) Geometrical mean values between Draupne and Sognefjord formations of inverted AI cube showing the lateral impedance variation with the same random line. C) The inverted AI cross-section along the line A-A'. The top Draupne, Sognefjord, and Fensfjord Formation horizons are shown for reference.

Basin, North Texas. There are significant differences in depositional and diagenetic processes between the studied caprocks (Draupne and Heather formations) and the Barnett Shale. Therefore, the range of Young's modulus and Poison's ratio used by Grieser and Bray (2007) to define ductile and brittle regions are working well in their studied basin but are not representative of our study area. Similarly, the mineralogy based brittleness increment trend proposed by Perez and Marfurt (2014) is specific for the Barnett shale and not demonstrated the trend observed in the studied caprocks. This indicates a basin specific brittleness analysis is needed to characterize the geomechanical behavior of the caprocks.

Caprocks with high values of elastic properties (i.e., AI, E, μρ, and λρ) tend to be stiffer though PR do not show a significant variation with change in brittleness values. However, the very soft ductile caprock cluster exhibits significantly high PR and low E values. The elastic properties based stiffness might be a tool to evaluate qualitative measures of the ability of the caprock to deform, but the whole procedure is much more complicated. For example, the well 35/11–4, which has stiff (Figs. 12 and 13) caprock (i.e., high values of elastic properties) with low clay fraction and a high percentage of stiff minerals (Table 3), acted as an effective caprock overlying a discovery. Although certain minerals (i.e., stiff mineral fraction) and processes (i.e., depositional and diagenetic) may enhance acoustic and geomechanical properties of the caprock (Fig. 22), the deformation of the rock is controlled by many other factors including clay type, microstructure, and distribution of minerals within the matrix, etc.

The complex nature of geomechanical properties of caprocks defines the sealing efficiency of any reservoir-caprock pairs. Considering all the analyses performed in this study, the Draupne Formation is in the realm of ductile caprock (BI's $< \sim 0.5$), which indicates significant sealing potential in the studied area. However, the thickness variation may raise questions regarding caprock failure, which is already answered by Troll West Field, where the studied caprocks are thin or not present, but overburden rocks acted as a potential cap. In contrast, the Heather Formation tends to be less ductile (higher BI's than Draupne) but can be an effective seal combined with the Draupne Formation (Fig. 18).

5.4. Implication

The relation between mineralogical composition and elastic properties within the organic-rich caprock shales allows us to estimate geomechanical properties from seismic data (Fig. 21). However, the complex nature of the geomechanical properties of caprock makes it challenging to approximate it. For example, the caprock properties (i.e., acoustic and geomechanical) of MC well 35/11–4 and CC well 35/11-6 plot in high Vp-density zone where the former well possesses effective caprock that contains gas in the underlying reservoir. In contrast, the latter well failed to find commercial hydrocarbon (only oil shows) considering minimal stress changes due to exhumation (i.e., ~150 m). The data from the other two wells containing the effective caprock, i.e., 31/5–2 (MC) and 35/10–1 (CC), show soft (low to intermediate Vp & density) ductile (Fig. 23). This type of distribution of acoustic properties

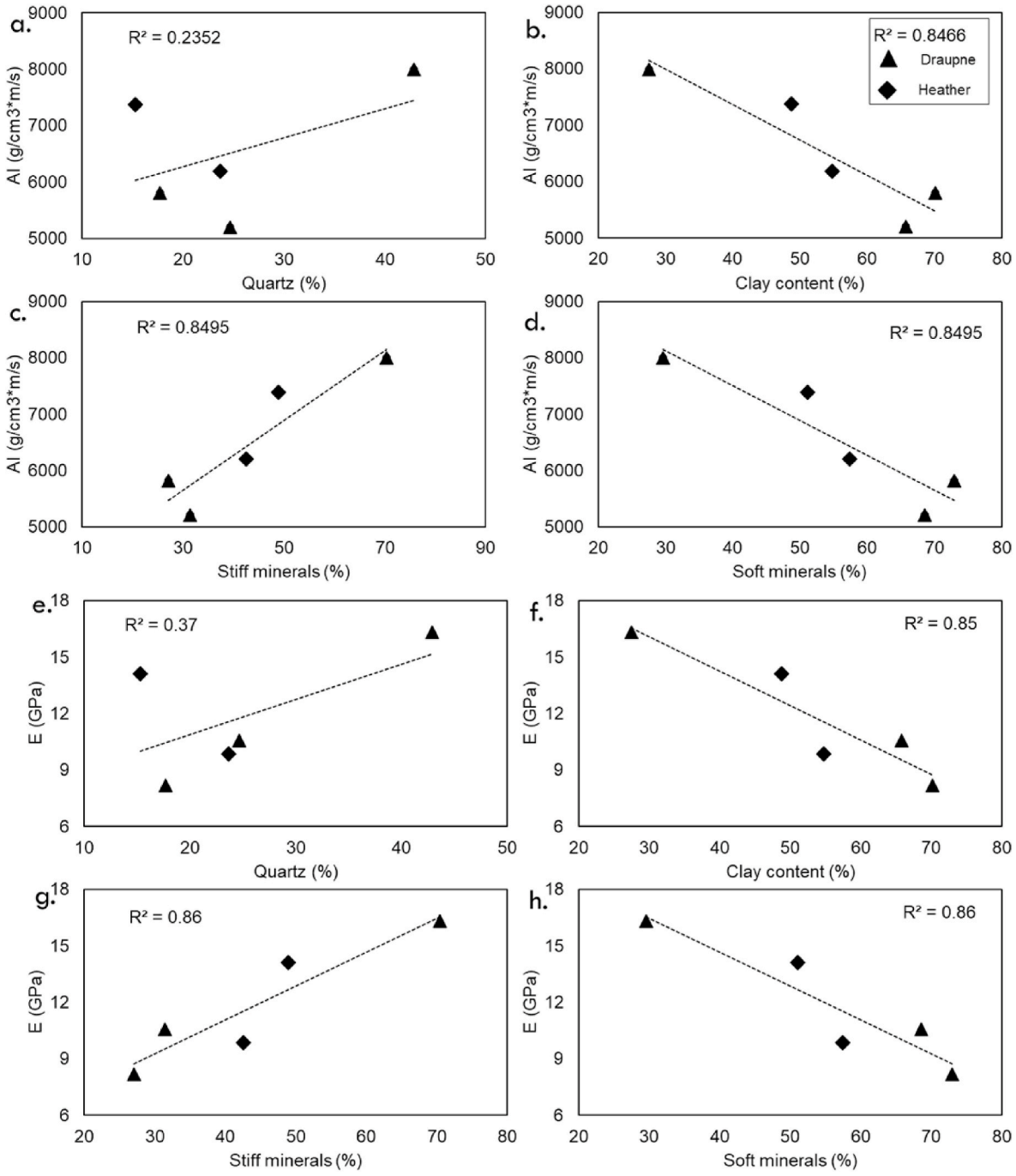

Fig. 22. Cross-plots of Draupne and Heather formations data points from the studied wells show the correlation of a) AI versus quartz, b) clay, c) stiff minerals, d) ductile minerals, e) E versus quartz, f) clay, g) stiff minerals and h) ductile minerals. Stiff mineral assemblages are composed of quartz, feldspar, pyrite, and carbonate, while ductile minerals consist of total clay and total organic content (TOC).

makes it very challenging to identify the effective seal rocks from seismic data. Therefore, an integrated approach (i.e., petrographic, petrophysical, seismic inversion, and laboratory analysis) is needed to get a detailed characterization of caprocks with their sealing effectiveness; otherwise, it might be misleading sometimes. Moreover, the caprock properties are not possible to describe by a single parameter such as stiffness or brittleness; instead, it is controlled by a combination of factors including in situ stress condition, pore-throat size, matrix permeability, capillary pressure, the existence of natural fractures, manner of well completion, as well as rock properties such as elastic moduli and mineralogy (Yang et al., 2013).

6. Conclusions

Depositional and diagenetic processes and their effect on caprock elastic and geomechanical properties were assessed. The critical observation of this study are as follows:

- The high energy NE-SW trend following the Troll fault zone separates the study area into two paleo-depositional regions where the NW part has high energy silts deposited compared to fine-grained clay-bearing zones in the SE part. However, in the NW and SW corners of the study area (far from the coastal plain), soft clay content and a higher percentage of organic matter are found.

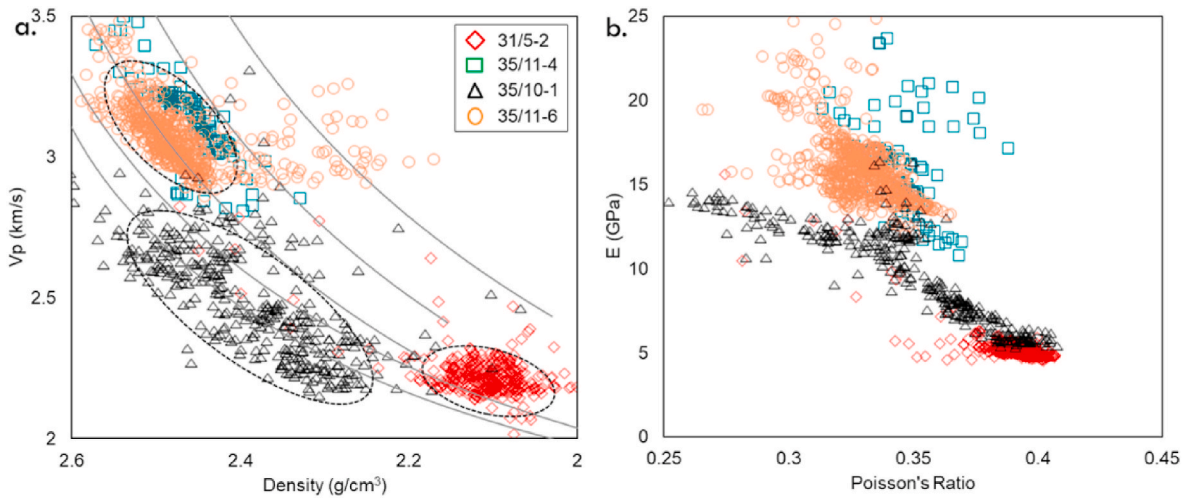

Fig. 23. Draupne Formation data points from wells 31/5–2, 35/10–1, 35/11–4, and 35/11–6 cross-plotted in a) the Vp-density template with reference curve adapted from Avseth et al. (2005) and b) E-PR template showing the increasing brittleness trend.

- Draupne and Heather formations in the study area showed a wide range of elastic and geomechanical properties. The data clustering irrespective of diagenetic variation makes it difficult to assess the properties from surface seismic.
- A stiff relationship is found between the rock mineralogical composition and caprock properties (i.e., elastic and geomechanical parameters).
- The mechanical properties of the studied caprocks appear to be ductile. However, Heather Formation is comparatively less ductile compared to Draupne Formation. The brittleness increment trend showed a significant difference with the previously published reference curves and increased with increasing AI, E, μρ, and λρ.
- There is considerable uncertainty involved in the estimation of TOC. However, the sparsely distributed (mostly immature) TOC within the study area has an insignificant impact on the geomechanical properties. The geomechanical properties of caprocks are complex, and further work is needed to quantify the TOC effect.

CRediT authorship contribution statement

Md Jamilur Rahman: Conceptualization, Methodology, Formal analysis, Investigation, Writing - original draft, Writing - review & editing, Visualization. **Manzar Fawad:** Conceptualization, Writing - review & editing, Supervision. **Nazmul Haque Mondol:** Conceptualization, Writing - review & editing, Supervision, Project administration, Funding acquisition.

Declaration of competing interest

The authors declare that they have no known competing financial interests or personal relationships that could have appeared to influence the work reported in this paper.

Acknowledgments

We are grateful for the financial support provided by the Research Council of Norway for the OASIS (Overburden Analysis and Seal Integrity Study for CO_2 Sequestration in the North Sea) project (NFR-CLIMIT project #280472). We are indebted to the additional funding and data provided by Norwegian Petroleum Directorate (NPD), Gassnova, Equinor, and Total. Academic software licenses have been provided by Lloyd's Register for Interactive Petrophysics and Schlumberger for Petrel.

Appendix A. Supplementary data

Supplementary data to this article can be found online at https://doi.org/10.1016/j.marpetgeo.2020.104665.

References

Alfred, D., Vernik, L., 2013. A new petrophysical model for organic shales. Petrophysics 54 (3), 240–247.
Alzahabi, A., AlQahtani, G., Soliman, M.Y., Bateman, R.M., Asquith, G., Vadapalli, R., 2015. June. Fracturability index is a mineralogical index: a new approach for fracturing decision. In: SPE Saudi Arabia Section Annual Technical Symposium and Exhibition. Society of Petroleum Engineers.
Anell, I., Thybo, H., Artemieva, I.M., 2009. Cenozoic uplift and subsidence in the North Atlantic region: geological evidence revisited. Tectonophysics 474 (1–2), 78–105. https://doi.org/10.1016/j.tecto.2009.04.006.
Aoudia, K., Miskimins, J.L., Harris, N.B., Mnich, C.A., 2010. January. Statistical analysis of the effects of mineralogy on rock mechanical properties of the Woodford shale and the associated impacts for hydraulic fracture treatment design. In: 44th US Rock Mechanics Symposium and 5th US-Canada Rock Mechanics Symposium. American Rock Mechanics Association.
Avseth, P., Mukerji, T., Mavko, G., 2005. Quantitative Seismic Interpretation: Applying Rock Physics Tools to Reduce Interpretation Risk. Cambridge University Press, New York.
Baig, I., Faleide, J.I., Mondol, N.H., Jahren, J., 2019. Burial and exhumation history controls on shale compaction and thermal maturity along the Norwegian North Sea basin margin areas. Mar. Petrol. Geol. 104, 61–85. https://doi.org/10.1016/j.marpetgeo.2019.03.010.
Bjørlykke, K., 2015. Petroleum migration. In: Bjørlykke, K. (Ed.), Petroleum Geoscience. From Sedimentary Environments to Rock Physics, second ed. Springer-Verlag Berlin Heidelberg, pp. 373–384. https://doi.org/10.1007/978-3-642-34132-8.
Carcione, J.M., 2000. A model for seismic velocity and attenuation in petroleum source rocks an Acoustic Model for Petroleum Source Rocks. Geophysics 65 (4), 1080–1092. https://doi.org/10.1190/1.1444801.
Carcione, J.M., Avseth, P., 2015. Rock-physics templates for clay-rich source rocks RPTs for clay-rich source rocks. Geophysics 80 (5), D481–D500. https://doi.org/10.1190/geo2014-0510.1.
Chen, J., Zhang, G., Chen, H., Yin, X., 2014. The Construction of Shale Rock Physics Effective Model and Prediction of Rock Brittleness. *2014*. SEG Technical Program Expanded Abstracts, pp. 2861–2865.
Dang, S.T., Sondergeld, C.H., Rai, C.S., 2016. A new approach to measuring organic density. Petrophysics 57 (2), 112–120.
Davis, D., Reynolds, S.J., 1996. Structural Geology of Rocks and Regions, second ed. Wiley and Sons.
Eberhardt, E., Stead, D., Stimpson, B., 1999. Quantifying progressive pre-peak brittle fracture damage in rock during uniaxial compression. Int. J. Rock Mech. Min. Sci. 36 (3), 361–380. https://doi.org/10.1016/S0148-9062(99)00019-4.
Emery, D., Myers, K., 1996. Sequence Stratigraphy. John Wiley & Sons.
Faerseth, R.B., 1997. Interaction of permo-triassic and jurassic extensional fault-blocks during the development of the northern North sea. Oceanogr. Lit. Rev. 7 (44), 710.
Faleide, J.I., Bjørlykke, K., Gabrielsen, R.H., 2015. Geology of the Norwegian continental shelf. Chapter 25 from the book. "Bjørlykke, K Petrol. Geosci.: From Sedimentary Environments to Rock Physics" 603–637, 2nd edition.
Fawad, M. & Mondol, N. H., 2020. (Proposed unpublished brittleness equation).

Fossen, H., Hurich, C.A., 2005. The hardangerfjord shear zone in SW Norway and The north sea: a large-scale low-angle shear zone in the caledonian crust. J. Geol. Soc. 162 (4), 675–687. https://doi.org/10.1144/0016-764904-136.
Gabrielsen, R.H., Faleide, J.I., Pascal, C., Braathen, A., Nystuen, J.P., Etzelmuller, B., O'Donnell, S., 2010. Latest Caledonian to present tectonomorphological development of southern Norway. Mar. Petrol. Geol. 27 (6), 1290–1295. https://doi.org/10.1016/j.marpetgeo.2009.06.004.
Gale, J.F., Reed, R.M., Holder, J., 2007. Natural fractures in the Barnett Shale and their importance for hydraulic fracture treatments. AAPG Bull. 91 (4), 603–622. https://doi.org/10.1306/11010606061.
Glorioso, J.C., Rattia, A., 2012. March. Unconventional reservoirs: basic petrophysical concepts for shale gas. cp-285. In: SPE/EAGE European Unconventional Resources Conference & Exhibition-From Potential to Production. European Association of Geoscientists & Engineers. https://doi.org/10.3997/2214-4609-pdb.285.spe153004.
Grieser, W.V., Bray, J.M., 2007. January. Identification of production potential in unconventional reservoirs. In: Production and Operations Symposium. Society of Petroleum Engineers.
Handin, J., Hager Jr., R.V., 1957. Experimental deformation of sedimentary rocks under confining pressure: tests at room temperature on dry samples. AAPG (Am. Assoc. Pet. Geol.) Bull. 41 (1), 1–50. https://doi.org/10.1306/5CEAE5FB-16BB-11D7-8645000102C1865D.
Hansen, J.A., Mondol, N.H., Fawad, M., 2019. Organic content and maturation effects on elastic properties of source rock shales in the Central North Sea. Interpretation 7 (2), T477–T497. https://doi.org/10.1190/INT-2018-0105.1.
Hart, B.S., Macquaker, J.H., Taylor, K.G., 2013. Mudstone ("shale") depositional and diagenetic processes: implications for seismic analyses of source-rock reservoirs. Interpretation 1 (1), B7–B26. https://doi.org/10.1190/INT-2013-0003.1.
Hunt, J.M., 1996. Petroleum geology and geochemistry. emanandCompanyt SanFrancisco 26i (5), 273, 197g.
Jarvie, D.M., Hill, R.J., Ruble, T.E., Pollastro, R.M., 2007. Unconventional shale-gas systems: the Mississippian Barnett Shale of north-central Texas as one model for thermogenic shale-gas assessment. AAPG Bull. 91 (4), 475–499. https://doi.org/10.1306/12190606068.
Jin, X., Shah, S.N., Roegiers, J.C., Zhang, B., 2014. February. Fracability evaluation in shale reservoirs-an integrated petrophysics and geomechanics approach. In: SPE Hydraulic Fracturing Technology Conference. Society of Petroleum Engineers.
Johnson, J.W., Nitao, J.J., Morris, J.P., 2004. Reactive transport modeling of cap-rock integrity during natural and engineered CO2 storage. Carbon dioxide capture for storage in deep geologic formations 2, 787.
Jordt, H., Faleide, J.I., Bjørlykke, K., Ibrahim, M.T., 1995. Cenozoic sequence stratigraphy of the central and northern North Sea Basin: tectonic development, sediment distribution and provenance areas. Mar. Petrol. Geol. 12 (8), 845–879. https://doi.org/10.1016/0264-8172(95)98852-V.
Larionov, V.V., 1969. Radiometry of Boreholes. Nedra, Moscow, p. 127.
Marcussen, Ø., Thyberg, B.I., Peltonen, C., Jahren, J., Bjørlykke, K., Faleide, J.I., 2009. Physical properties of Cenozoic mudstones from the northern North Sea: impact of clay mineralogy on compaction trends. AAPG Bull. 93 (1), 127–150. https://doi.org/10.1306/08220808044.
Meyer, B.L., Nederlof, M.H., 1984. Identification of source rocks on wireline logs by density/resistivity and sonic transit time/resistivity crossplots. AAPG Bull. 68 (2), 121–129. https://doi.org/10.1306/AD4609E0-16F7-11D7-8645000102C1865D.
Mondol, N.H., Bjørlykke, K., Jahren, J., Høeg, K., 2007. Experimental mechanical compaction of clay mineral aggregates—changes in physical properties of mudstones during burial. Mar. Petrol. Geol. 24 (5), 289–311. https://doi.org/10.1016/j.marpetgeo.2007.03.006.
Mondol, N.H., 2009. Porosity and Permeability Development in Mechanically Compacted Silt-Kaolinite Mixtures. SEG Technical Program Expanded Abstracts, pp. 2139–2143. *2009*.
Mullen, M.J., Roundtree, R., Turk, G.A., 2007. January. A composite determination of mechanical rock properties for stimulation design (what to do when you don't have a sonic log). In: Rocky Mountain Oil & Gas Technology Symposium. Society of Petroleum Engineers.
Norton, D.L., 1984. Theory of hydrothermal systems. Annu. Rev. Earth Planet Sci. 12 (1), 155–177.
Nygård, R., Gutierrez, M., Bratli, R.K., Høeg, K., 2006. Brittle–ductile transition, shear failure and leakage in shales and mudrocks. Mar. Petrol. Geol. 23 (2), 201–212. https://doi.org/10.1016/j.marpetgeo.2005.10.001.
Passey, Q.R., Creaney, S., Kulla, J.B., Moretti, F.J., Stroud, J.D., 1990. A practical model for organic richness from porosity and resistivity logs. AAPG Bull. 74 (12), 1777–1794.
Peters, K.E., 1986. Guidelines for evaluating petroleum source rock using programmed pyrolysis. AAPG Bull. 70 (3), 318–329.
Perez Altamar, R., Marfurt, K., 2014. Mineralogy-based brittleness prediction from surface seismic data: application to the Barnett Shale. Interpretation 2 (4), T1–T17. https://doi.org/10.1190/INT-2013-0161.1.
Rickman, R., Mullen, M.J., Petre, J.E., Grieser, W.V., Kundert, D., 2008. January. A practical use of shale petrophysics for stimulation design optimization: all shale plays are not clones of the Barnett Shale. In: SPE Annual Technical Conference and Exhibition. Society of Petroleum Engineers.
Roberts, A.M., Yielding, G., Kusznir, N.J., Walker, I., Dorn-Lopez, D., 1993. January. Mesozoic extension in the North Sea: constraints from flexural backstripping, forward modelling and fault populations. In: Geological Society, London, Petroleum Geology Conference Series, vol. 4. Geological Society of London, pp. 1123–1136. https://doi.org/10.1144/0041123. No. 1.
Roberts, A.M., Kusznir, N.J., Yielding, G., Beeley, H., 2019. Mapping the bathymetric evolution of the Northern North Sea: from Jurassic synrift archipelago through Cretaceous-Tertiary post-rift subsidence. Petrol. Geosci. 25 (3), 306–321. https://doi.org/10.1144/petgeo2018-066.
Rybacki, E., Meier, T., Dresen, G., 2016. What controls the mechanical properties of shale rocks?–Part II: Brittleness. J. Petrol. Sci. Eng. 144, 39–58. https://doi.org/10.1016/j.petrol.2016.02.022.
Shell, U.K., 2014. Peterhead CCS project: geomechanics report. Revision-K02, doc. No. PCCS-05-PT-ZP-9025-00004.
Sharma, R.K., Chopra, S., 2012. New attribute for determination of lithology and brittleness. In: SEG Technical Program Expanded Abstracts 2012. Society of Exploration Geophysicists, pp. 1–5.
Slatt, R., 2011. Important geological properties of unconventional resource shales. Open Geosci. 3 (4), 435–448.
Slatt, R.M., Abousleiman, Y., 2011. Merging sequence stratigraphy and geomechanics for unconventional gas shales. Lead. Edge 30 (3), 274–282. https://doi.org/10.1190/1.3567258.
Stewart, D.J., Schwander, M., Bolle, L., 1995. Jurassic Depositional Systems of the Horda Platform, Norwegian North Sea: Practical Consequences of Applying Sequence Stratigraphic Models, vol. 5. Norwegian Petroleum Society Special Publications, pp. 291–323. https://doi.org/10.1016/S0928-8937(06)80073-1.
Storvoll, V., Bjørlykke, K., Mondol, N.H., 2005. Velocity-depth trends in mesozoic and cenozoic sediments from the Norwegian shelf. AAPG Bull. 89 (3), 359–381. https://doi.org/10.1306/10150404033.
Taylor, K.G., Macquaker, J.H., 2011. Iron minerals in marine sediments record chemical environments. Elements 7 (2), 113–118.
Thyberg, B., Jahren, J., Winje, T., Bjørlykke, K., Faleide, J.I., 2009. From mud to shale: rock stiffening by micro-quartz cementation. First Break 27 (2). https://doi.org/10.3997/1365-2397.2009003.
Van Wagoner, J.C., Posamentier, H.W., Mitchum, R.M.J., Vail, P.R., Sarg, J.F., Loutit, T.S., Hardenbol, J., 1988. An overview of the fundamentals of sequence stratigraphy and key definitions.
Verdon, J.P., Kendall, J.M., Stork, A.L., Chadwick, R.A., White, D.J., Bissell, R.C., 2013. Comparison of geomechanical deformation induced by megatonne-scale CO2 storage at Sleipner, Weyburn, and in Salah. Proc. Natl. Acad. Sci. Unit. States Am. 110 (30), E2762–E2771. https://doi.org/10.1073/pnas.1302156110.
Vernik, L., Landis, C., 1996. Elastic anisotropy of source rocks: implications for hydrocarbon generation and primary Migration1. AAPG Bull. 80 (4), 531–544. https://doi.org/10.1306/64ED8836-1724-11D7-8645000102C1865D.
Vernik, L., Milovac, J., 2011. Rock physics of organic shales. Lead. Edge 30 (3), 318–323. https://doi.org/10.1190/1.3567263.
Walles, F., 2004. A new method to help identify unconventional targets for exploration and development through integrative analysis of clastic rock property fields.
Wang, F.P., Gale, J.F., 2009. Screening criteria for shale-gas systems.
Whipp, P.S., Jackson, C.L., Gawthorpe, R.L., Dreyer, T., Quinn, D., 2014. Normal fault array evolution above a reactivated rift fabric; a subsurface example from the northern Horda Platform, Norwegian North Sea. Basin Res. 26 (4), 523–549.
Yang, Y., Sone, H., Hows, A., Zoback, M.D., 2013. January. Comparison of brittleness indices in organic-rich shale formations. In: 47th US Rock Mechanics/geomechanics Symposium. American Rock Mechanics Association.
Zhang, D., Ranjith, P.G., Perera, M.S.A., 2016. The brittleness indices used in rock mechanics and their application in shale hydraulic fracturing: a review. J. Petrol. Sci. Eng. 143, 158–170. https://doi.org/10.1016/j.petrol.2016.02.011.